

# Majorana physics in braiding and transport

Zur Erlangung des akademischen Grades eines  
DOKTORS DER NATURWISSENSCHAFTEN (Dr. rer. nat.)

von der KIT-Fakultät für Physik  
des Karlsruher Instituts für Technologie (KIT)  
angenommene

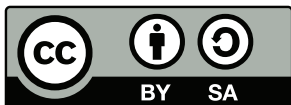
DISSERTATION

von

Stefan Backens, M. Sc.

Tag der mündlichen Prüfung: 17. Juli 2020

Referent: Prof. Dr. Alexander Shnirman  
Korreferent: Prof. Dr. Alexander Mirlin



This work is licensed under a Creative Commons  
„Attribution-ShareAlike 4.0 International“ licence.

# Introduction

The concept of Majorana fermions, developed by Italian physicist *Ettore Majorana*, originates from particle physics, where it provides a field-theoretic description of charge-neutral fermionic particles. The discovery of oscillations between different neutrino flavours (2015 Nobel Prize in Physics) has boosted interest in Majorana theory as one possible way to add neutrino masses to the Standard Model. The existence of Majorana mass terms would imply that the fermion number is not a conserved quantity.

In condensed-matter physics, on the other hand, fermionic systems with non-conserved particle number are well known from the mean-field theory of *superconductivity*, where all excitations have a Majorana character. This property is a manifestation of the redundancy (Nambu doubling) that is needed to treat a superconductor like an ordinary system of free fermions. The gauge-dependent nature of the superconducting order parameter means that, in contrast to the concept from particle theory, Majorana modes in a superconductor are not restricted to being electrically neutral.

Majorana states of lower dimensionality, in particular, have drawn interest in condensed-matter research: *Majorana zero modes*, bound states of exponential localisation, may be useful as topologically protected degrees of freedom for quantum-computation applications, as they are not susceptible to some decoherence processes caused by perturbations and imperfections of the system. One-dimensional *Majorana edge modes* enrich the field of effectively 1D physics and offer the possibility of probing quantum properties in interferometric studies.

Suitability for topological quantum computation was first predicted for zero-energy Majorana bound states hosted by vortices in a p-wave superconductor [1]. A simpler, 1D model of a topological superconducting system is given by the *Kitaev chain* [2], which provides Majorana zero modes localised at both ends. As the model is strictly one-dimensional, it has a direct equivalent, via *Jordan–Wigner transformation*, in a spin- $\frac{1}{2}$  chain with Ising coupling. Although the character of the spin system differs substantially from the fermionic one due to the non-locality involved in the transformation, it still has the potential to emulate behaviour of the fermion chain.

For the appearance of one-dimensional edges, a system with at least two dimensions is required. A three-dimensional *topological insulator*, for instance, features gapless electronic states on the surface, which acts as an effectively 2D system. Edge modes of Majorana character may arise at boundary lines between a surface region gapped by a superconductor and a magnetically influenced area, or in line junctions between two superconducting regions [3]. The gapless surface states will generally have a contribution to the Josephson current flowing between two superconductors that are tunnel-coupled to the surface.

Both the spin equivalent of the Kitaev chain and superconducting fermionic systems with topological Majorana modes are studied in this thesis, which consists of five chapters:

- The first chapter introduces fundamental concepts that are relevant, in particular the Jordan–Wigner transformation, the toy model of the Kitaev chain, Majorana zero modes and their use in *topological braiding*, and protected surface states in a topological insulator.

- The second chapter presents a generalised Jordan–Wigner transformation which provides a locality-preserving mapping between *tree structures* of spins and of fermions. The extension uses additional spins to mediate the coupling between one-dimensional chains and allows for the translation of Majorana braiding into a spin system.
- For a mesoscopic superconducting island hosting two Majorana zero modes, the onset, due to charging energy, of *correlations* between the electrical currents at two tunnel contacts coupled to the Majorana modes is analysed in the third chapter.
- In the fourth chapter, a *Josephson junction* between two superconductors on a topological-insulator surface is considered and the current–phase relation is calculated for the contributions of bound states and scattering states on the surface to the Josephson current.
- Finally, the thesis is concluded by a *summary* with some outlook on further research potential.

# Contents

<b>Introduction</b>	<b>iii</b>
<b>1 Fundamentals</b>	<b>1</b>
1.1 Jordan–Wigner transformation . . . . .	1
1.2 Majorana operators and non-local zero modes . . . . .	2
1.3 Kitaev toy model of a topological superconductor . . . . .	3
1.4 Topological braiding with Majorana modes . . . . .	5
1.5 Superconducting Majorana structure on a topological insulator . . . . .	7
<b>2 Jordan–Wigner transformations for tree structures</b>	<b>9</b>
2.1 Spin–fermion mapping beyond 1D . . . . .	9
2.2 Geometry and notations . . . . .	10
2.3 Free fermions and 3-spin couplings . . . . .	11
2.4 XY spin system and fermionic Kondo model . . . . .	12
2.5 Majorana braiding and the spin representation . . . . .	13
2.6 Conclusion . . . . .	14
<b>3 Current correlation in a Majorana system with charging energy</b>	<b>15</b>
3.1 Transport through Majorana modes . . . . .	15
3.2 Model . . . . .	15
3.3 Langevin equation . . . . .	16
3.4 Currents and correlations . . . . .	17
3.5 Low-energy limit . . . . .	18
3.6 Conclusion . . . . .	19
<b>4 Current–phase relation in a long topological Josephson junction</b>	<b>21</b>
4.1 Proximity effects on a topological insulator . . . . .	21
4.2 Electronic modes . . . . .	21
4.3 SNS case . . . . .	23
4.3.1 Scattering states . . . . .	23
4.3.2 Bound states . . . . .	24
4.3.3 Josephson current . . . . .	26
4.4 SMS case . . . . .	28
4.4.1 Scattering states . . . . .	28
4.4.2 Bound states . . . . .	28
4.4.3 Josephson current . . . . .	29
4.5 Zero-temperature results . . . . .	30
4.6 Conclusion . . . . .	33
<b>5 Summary and outlook</b>	<b>35</b>

<b>A Majorana braiding in spin representation</b>	<b>37</b>
A.1 Geometry . . . . .	37
A.2 Boundary translations . . . . .	38
A.3 Single-interval braiding . . . . .	39
A.4 Two-interval braiding . . . . .	42
<b>B Effective action and phase fluctuations</b>	<b>45</b>
B.1 Derivation of the effective action . . . . .	45
B.2 Fluctuation kernel and decoupling . . . . .	46
B.3 Low-energy evaluation of noise averages . . . . .	47
<b>C Details of the correlation calculation</b>	<b>49</b>
C.1 Current and correlation in the limit of large $\Gamma$ . . . . .	49
C.2 Further treatment of the zero-temperature case . . . . .	51
<b>D Supercurrent in a thermal state</b>	<b>53</b>
<b>E Current calculation via eigenmodes</b>	<b>55</b>
<b>List of Figures</b>	<b>59</b>
<b>Bibliography</b>	<b>61</b>
<b>Acknowledgements</b>	<b>63</b>

# 1

## Chapter 1

---

# Fundamentals

*This chapter is a short introduction of some fundamental concepts. The first part explains the definition and applications of the Jordan–Wigner transformation relating spin- $\frac{1}{2}$  systems to fermions. Fermionic Majorana operators do not only result from transforming spin components, as shown in the second part, but they can also arise as topologically protected degrees of freedom in a fermionic system like the Kitaev chain, which is presented in the third part. Protected Majorana states have non-Abelian braiding properties, discussed in the fourth part, which could be used for topological quantum computation. The last part describes Majorana modes as a more general feature of superconductors, which is of particular interest in combination with the protected surface states of a topological insulator.*

## 1.1 Jordan–Wigner transformation

The well-known transformation introduced by Jordan and Wigner [4] relates spin- $\frac{1}{2}$  operators to fermionic creation and annihilation operators. Thereby, it permits mapping a spin system to a fermionic one (and vice versa). For sets of fermionic operators  $c(j)$ ,  $c^\dagger(j)$  and spin raising/lowering operators

$$\sigma^\pm(j) = \frac{1}{2} \left[ \sigma^x(j) \pm i \sigma^y(j) \right] \quad (1.1)$$

derived from Pauli matrices  $\sigma^\alpha(j)$ , the Jordan–Wigner transformation can be defined as follows:

$$c(j) = \sigma^-(j) \cdot \prod_{k=1}^{j-1} \sigma^z(k) \quad (1.2a)$$

$$c^\dagger(j) = \sigma^+(j) \cdot \prod_{k=1}^{j-1} \sigma^z(k) . \quad (1.2b)$$

[By means of an additional spin rotation, components can be swapped, which may be expedient for some applications.]

To transform the commuting operators of various spins into anti-commuting fermionic operators, highly non-local string operators are used. In principle, the one-dimensional ordering required for the strings can be chosen arbitrarily. However, this transformation generally provides a locality-preserving mapping between Hamiltonians only for strictly one-dimensional systems.

In a one-dimensional chain, the Jordan–Wigner transformation can be used to map any local quadratic fermionic Hamiltonian into a local quadratic spin Hamiltonian:

$$H_0^F = \sum_j \mu_j c^\dagger(j) c(j) + \sum_j \left[ u_j c(j) c(j+1) + t_j c^\dagger(j) c(j+1) + \text{H. c.} \right] \quad (1.3a)$$

$$\xrightarrow{(1.2)} H^S = \sum_j \mu_j \frac{1 + \sigma^z(j)}{2} + \sum_j \left[ u_j \sigma^-(j) \sigma^-(j+1) - t_j \sigma^+(j) \sigma^-(j+1) + \text{H. c.} \right], \quad (1.3b)$$

where the relation

$$\sigma^+(j) \sigma^-(j) = \frac{1}{2} \left[ 1 + \sigma^z(j) \right] \quad (1.4)$$

was used. Conversely, a 1D spin chain with XY coupling between nearest neighbours and local transversal fields is mapped to a free fermionic Hamiltonian.

## 1.2 Majorana operators and non-local zero modes

For every pair of fermionic creation operator  $c^\dagger(j)$  and annihilation operator  $c(j)$ , we can define two Majorana operators

$$\gamma(2j-1) = c(j) + c^\dagger(j), \quad \gamma(2j) = -i \left[ c(j) - c^\dagger(j) \right]. \quad (1.5)$$

The operators are Hermitian (or *real*) and they fulfill an anti-commutation relation

$$\left\{ \gamma(j), \gamma(k) \right\} = 2 \delta_{jk}, \quad (1.6)$$

similar to the usual (complex) fermion operators.<sup>1</sup> The fermionic anti-commutation relation leads to the special property that an arbitrary pair of Majorana operators can be recombined,

$$f = \frac{\gamma(j) + i\gamma(k)}{2}, \quad f^\dagger = \frac{\gamma(j) - i\gamma(k)}{2}, \quad (1.7)$$

(for  $j \neq k$ ) to a new complex fermion with occupation

$$f^\dagger f = \frac{1 + i\gamma(j)\gamma(k)}{2}. \quad (1.8)$$

As  $\gamma(j)$  are linear combinations of the original fermionic operators, a quadratic Hamiltonian consisting of Majorana operators describes a system of free fermions. An interesting fermionic Hamiltonian results from using the Jordan–Wigner transformation (1.2) for the new operators,

$$\gamma(2j-1) = \sigma^x(j) \cdot \prod_{k=1}^{j-1} \sigma^z(k) \quad (1.9a)$$

$$-\gamma(2j) = \sigma^y(j) \cdot \prod_{k=1}^{j-1} \sigma^z(k), \quad (1.9b)$$

---

<sup>1</sup>Alternatively, Majorana operators can be defined with an additional factor of  $1/\sqrt{2}$ , which results in an anti-commutator of  $\delta_{jk}$ , like the one for complex fermion operators.

on a ferromagnetic Ising spin chain ( $J > 0$ ) of length  $L$ :

$$H_{\text{Ising}}^{\text{S}} = -J \sum_{j=1}^{L-1} \sigma^x(j) \sigma^x(j+1) \quad (1.10a)$$

$$\longrightarrow H^{\text{F}} = J \sum_{j=1}^{L-1} i \gamma(2j) \gamma(2j+1) . \quad (1.10b)$$

Considering the fermionic operators for a 1D chain of length  $L$ , we notice that two Majorana operators do not appear in  $H^{\text{F}}$ . Therefore,  $\gamma(1)$  and  $\gamma(2L)$  form a non-local fermionic zero mode.

### 1.3 Kitaev toy model of a topological superconductor

A fermionic toy model capable of reproducing the Hamiltonian (1.10b) was proposed by Kitaev [2]. The starting point is a one-dimensional, (effectively) spinless chain of  $L$  fermions with chemical potential  $\mu$ , superconducting order parameter  $\Delta = |\Delta| e^{i\theta}$  and nearest-neighbour hopping amplitude  $w$ :

$$H_{\mu} = \sum_{j=1}^{L-1} \left[ -w c^{\dagger}(j) c(j+1) + \Delta c(j) c(j+1) + \text{H. c.} \right] - \mu \sum_{j=1}^L \left[ c^{\dagger}(j) c(j) - \frac{1}{2} \right] . \quad (1.11)$$

Redefining the Majorana operators to account for the superconducting phase,

$$c(j) = \frac{\gamma(2j-1) + i \gamma(2j)}{2} e^{i\theta} , \quad (1.12)$$

we now consider the special case of  $|\Delta| = w$  and obtain the Majorana representation:

$$H_{\mu} = w \sum_{j=1}^{L-1} i \gamma(2j) \gamma(2j+1) - \frac{\mu}{2} \sum_{j=1}^L i \gamma(2j-1) \gamma(2j) . \quad (1.13)$$

In this representation, the Hamiltonian  $H_{\mu}$  consists of two different kinds of Majorana pairings: The two Majorana operators of the same fermionic site are coupled by the chemical potential  $\mu$ , while  $w$  is the coefficient for pairs of Majorana operators from neighbouring sites (Fig. 1.1).

For a vanishing chemical potential,  $\gamma(1)$  and  $\gamma(2L)$  are *Majorana zero modes*, and the Hamiltonian  $H_{\mu=0}$  corresponds to the Ising chain (1.10a) with  $w = J$ . Due to the non-locality of the transformation, however, the ground-state degeneracy in the fermionic system is completely different from the Ising Hamiltonian:

In the spin system, the two ferromagnetic ground states can be distinguished by a local measurement of any spin. In contrast, this information can only be determined by accessing the two operators at distant ends of the topological fermion chain, providing a topological protection against local perturbations for this degree of freedom. This difference between topological and non-topological order has been elaborated in Ref. [5]; it is visualised for the ground states as well as elementary excitations in Fig. 1.2.

A physical realisation of the Hamiltonian (1.11) is possible by applying a magnetic field to a semi-conducting wire with spin-orbit coupling and proximity-induced superconductivity [6], as pictured in Fig. 1.3. If the chemical potential  $\mu$  is finite, there is no perfect zero mode. But in the regime  $0 < |\mu| < 2|w|$ , Majorana modes of finite extent are localised at the ends of the chain, and their overlap and energy are suppressed exponentially in the length  $L$  [2].

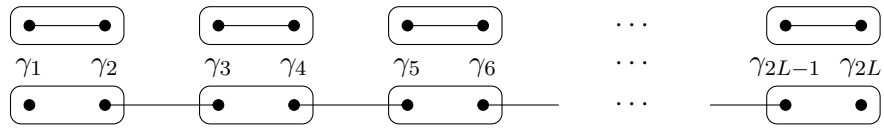


**Figure 1.1:** There are two different kinds of quadratic Majorana terms in the Hamiltonian (1.13) of the Kitaev chain [2]. The chemical potential  $\mu$  pairs the two Majorana operators of a single fermionic site (upper part). In contrast, the combination of superconducting and hopping terms effects a pairing between Majorana operators of neighbouring sites, leaving unpaired the two operators at the ends of the chain (lower part). Diagram inspired by Ref. [2].

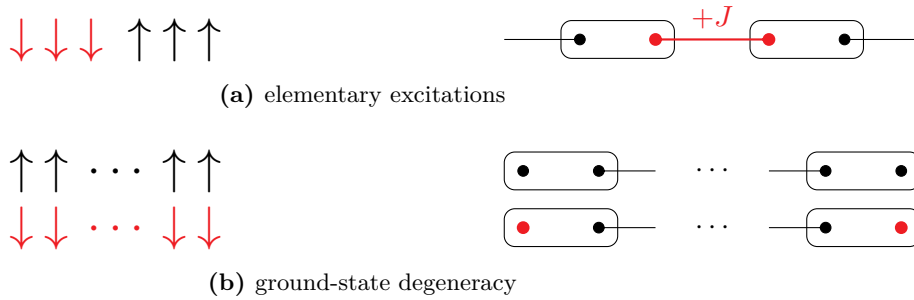


**Figure 1.2:** As the Jordan–Wigner transformation is non-local, it relates two very different kinds of order. In the ferromagnetic Ising chain (on the left), the lowest excitations are domain walls (a), and a measurement of a single spin is sufficient to distinguish the degenerate ground states (b). In the topological fermion chain (on the right), localised fermionic modes are the elementary excitations (a); due to the non-locality of the zero mode, in contrast, the ground states cannot be distinguished by any local measurement (b).

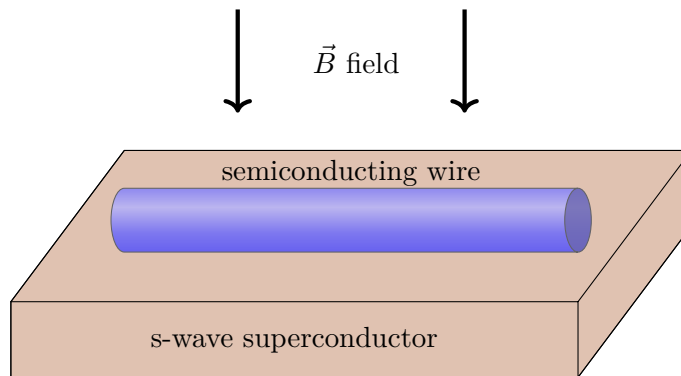


**Figure 1.3:** Schematic picture of a topological wire (inspired by Ref. [6]). A semiconducting wire with strong spin–orbit coupling can be driven into the topologically superconducting phase of the Kitaev toy model (1.11) by a combination of a magnetic field and proximity to a superconductor with s-wave order parameter [6].

## 1.4 Topological braiding with Majorana modes

Many-particle wave functions should satisfy a symmetry under the interchange of indistinguishable particles. In a system with three (or more) spatial dimensions, bosonic and fermionic statistics are the only possibilities for this, because physically interchanging the same two particles twice is topologically equivalent to no change at all. Restricted to  $2D$ , however, multiple interchanges of two particles can be characterised by a well-defined topological property, the winding number. Thus, in addition to bosons and fermions, particles with *anyonic* statistics may exist in 2D systems. In the simplest case, interchanging identical particles introduces an arbitrary phase  $e^{i\theta}$  with  $\theta \neq 0, \pi$  (values for bosons and fermions). As multiple phase factors always commute, this implies Abelian anyons.

If there is a ground-state degeneracy in the presence of anyonic particles, interchanging different pairs of particles may effect non-commuting rotations in the subspace of degenerate ground states. For such *non-Abelian* anyons, interchange sequences, which are represented by elements of the *braid group*, can yield complex transformations of the system state. The result does not depend on the precise trajectories, but only on the topology of the braiding; a graphical representation for a simple braiding operation is shown in Fig. 1.4. Hence, systems with non-Abelian statistics may provide a platform for quantum computations with topologically protected gates (see Ref. [7] for a review on non-Abelian anyons and their potential use).

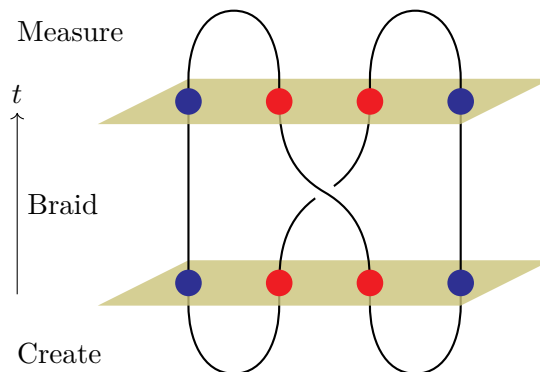


**Figure 1.4:** World-line diagram of a braiding operation with four particles. At first, two pairs of anyons are created (at the bottom of the diagram). Then, the middle ones of both pairs are interchanged. For *non-Abelian* anyons, this *braiding* results in a non-trivial transformation within the subspace of degenerate ground states. At the end, the state of the two particle pairs is measured. Picture inspired by Ref. [8].

In the following, we will focus on the non-Abelian anyons appearing in superconducting systems. They consist in a topological defect which protects a zero-energy Majorana mode. For Majorana zero modes in half-quantum vortices of p-wave superconductors (or single-quantum vortices in the spinless case), the unitary rotation was derived by Ivanov [1]: The operation

$$U = \exp\left(-\frac{\pi}{4} \gamma_A \gamma_B\right) = \frac{1 - \gamma_A \gamma_B}{\sqrt{2}} \quad (1.14)$$

is the effect of braiding two vortices with Majorana modes  $\gamma_A, \gamma_B$ . [The order of the two operators, or the sign of the rotation, depends on the chirality of the vortices and on the choice of branch cuts in the superconducting phase; a clockwise braiding features the opposite sign with respect to an anti-clockwise

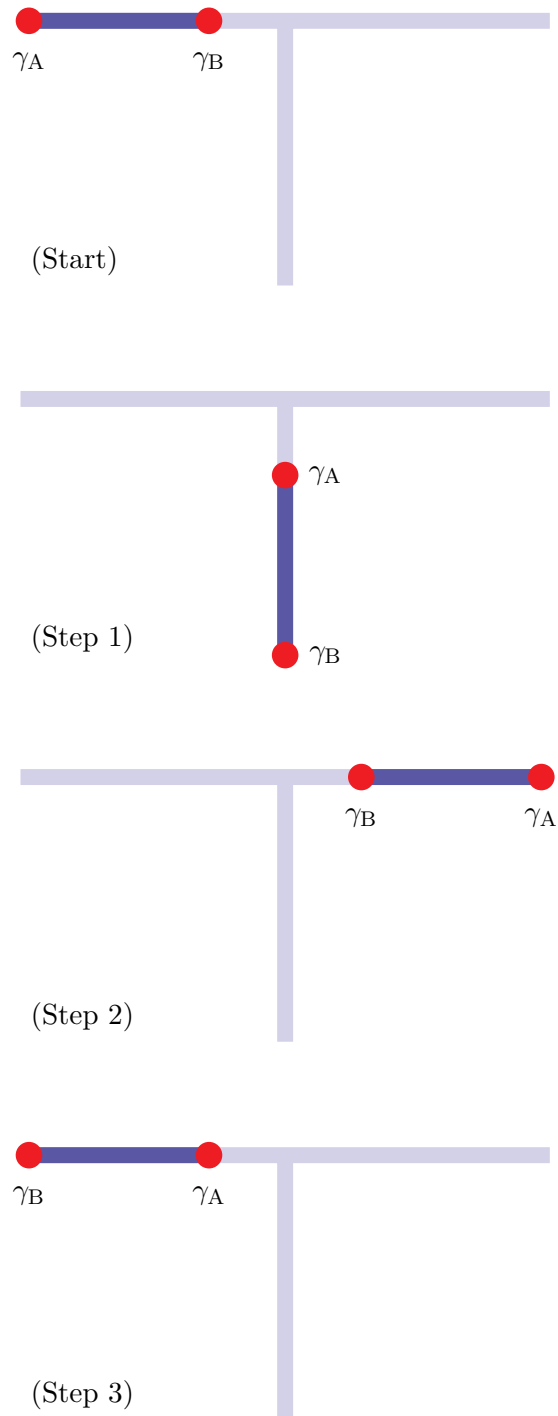


**Figure 1.5:** Majorana braiding in a T junction (picture inspired by Ref. [6]). Two Majorana zero modes at the boundaries of a topological interval (Sec. 1.3) are interchanged via adiabatical shifts of the interval boundaries. This can be effected by local control of the chemical potential and results in a rotation (1.14) of the system state [6].

braiding.] As should be expected, this transformation affects the Majorana operators involved,

$$\gamma_A \rightarrow U \gamma_A U^{-1} = \gamma_B , \quad (1.15a)$$

$$\gamma_B \rightarrow U \gamma_B U^{-1} = -\gamma_A , \quad (1.15b)$$

while leaving any other Majorana operator unchanged. Note that the anyonic statistics is not inherent to Majorana modes, which are fermionic in nature. The non-Abelian behaviour rather arises from the *topological structure* of the vortices protecting the zero modes.

In the topological phase of the Kitaev chain, or of the physical realisation in semiconducting wires, a boundary (of a topological part) of the system has the role of the topological defect. Braiding is obviously not possible in a strictly one-dimensional geometry, but in a network of topological wires: If the boundaries of the topological phase can be controlled by local tuning of the chemical potential with gates, Majorana braiding in the wire network is described by the same operator (1.14) as for Majorana vortices in 2D [6]. For a T geometry—the most elementary network—a braiding operation between two Majorana modes is depicted in Fig. 1.5.

The rotations described by Eq. (1.14) generate only the set of Clifford gates, which is a restricted class of quantum operations. Therefore, topological Majorana braiding needs to be complemented with unprotected operations to construct a universal set of quantum gates (see Ref. [9] for discussion and further references).

## 1.5 Superconducting Majorana structure on a topological insulator

Zero-energy Majorana modes that are hosted by topological defects in a superconductor have drawn much interest due to their non-Abelian braiding statistics, which could be used for topological quantum computation. The Majorana nature, however, is a general property of superconducting excitations, which is not restricted to protected zero modes. We will illustrate this fact using the example of induced superconductivity on the surface of a topological insulator, at first.

A *topological insulator* (TI) is characterised by an electronically insulating bulk, while there are protected gapless states at the boundaries. In a strong 3D TI, the two-dimensional surface provides ungapped boundary modes that are robust against disorder. They are, in the simplest case, described by a Hamiltonian for a single non-degenerate Dirac point:

$$h_{\text{surface}} = v \vec{p} \cdot \vec{\sigma} - \mu , \quad (1.16)$$

where  $\mu$  is the chemical potential,  $\vec{p}$  the 2D momentum operator and  $\vec{\sigma}$  characterises the spin. In presence of an s-wave superconductor, the Nambu notation  $\Psi = [\psi_{\uparrow}, \psi_{\downarrow}, \psi_{\downarrow}^{\dagger}, -\psi_{\uparrow}^{\dagger}]^T$  and Pauli matrices  $\vec{\tau}$  mixing particle and hole components can be used to incorporate a proximity-induced order parameter  $\Delta$ . Additionally, we allow for a time-reversal breaking Zeeman field  $M$  perpendicular to the surface (induced, e.g., by a magnetic insulator). The spectrum of the Hamiltonian  $H = \frac{1}{2} \Psi^{\dagger} h \Psi$  with

$$h = v \vec{p} \cdot \vec{\sigma} \tau^z - \mu \tau^z + [\Delta \tau^- + \Delta^* \tau^+] + M \sigma^z \quad (1.17)$$

is simply gapped out, for  $M = 0$ , by the *Majorana* mass  $\Delta$ :  $\epsilon_{\vec{k}} = \pm \sqrt{(\pm v |\vec{k}| - \mu)^2 + |\Delta|^2}$ . For  $\Delta = 0$ , the spectrum  $\epsilon_{\vec{k}} = \pm(\sqrt{v^2 k^2 + M^2} \pm \mu)$  has an effective *magnetic* gap only if  $|\mu| < |M|$ .

Let us consider an interface between a superconducting region,  $\Delta = \Delta_0 \theta(y)$ , and a half-plane with magnetic mass term,  $M = M_0 \theta(-y)$ . Fu and Kane [3] predicted that the boundary between the two

different gaps  $\Delta$  and  $M$  gives rise to one-dimensional *chiral* Majorana edge modes. They are chiral because there is only a single band of eigenmodes  $\gamma_k$ , with energy  $E_k = \hbar v k$ , while their Majorana nature means that states of positive and negative energy are not independent, but linked by the relation  $\gamma_k^\dagger = \gamma_{-k}$  [10].

*Non-chiral* Majorana modes arising in line junctions between two superconductors on a TI surface and trijunctions of these modes could be used to create and manipulate zero-dimensional Majorana *bound states*, similar to the zero modes in p-wave-superconducting vortices [3]. A setup of magnetic materials and superconductors deposited on the TI surface may also be useful as an interferometer for probing the one-dimensional Majorana edge states [10]. (Comprehensive reviews on one- and two-dimensional topological insulators, both in general and in connection with superconducting or magnetic phenomena, have been published in Refs. [8] and [11].)

Now we will discuss the generic properties of excitations in a superconductor. As shown in Ref. [12], their Majorana nature already follows from fundamental symmetries of the Bogoliubov–de Gennes Hamiltonian in superconducting mean-field theory:

$$H = \frac{1}{2} \int d^d r \, d^d r' \, \Psi^\dagger h \Psi . \quad (1.18)$$

First, the operator  $h$  conforms to the particle–hole symmetry

$$C^{-1} h C = -h^* \quad (1.19)$$

for a matrix  $C$ , with  $C C^* = 1$ . [For the surface Hamiltonian (1.17), e. g.,  $C = \sigma^y \tau^y$ .] As a result, for each positive-energy eigenmode  $\phi_n$  with  $h \phi_n = E_n \phi_n$ , there is a negative eigenmode  $\phi_{-n}$  with energy  $E_{-n} = -E_n$ . Pairs of positive and negative eigenmodes fulfill the symmetry relation

$$C \phi_n^* = \phi_{-n} . \quad (1.20)$$

The same kind of charge-conjugation symmetry is present in the Dirac equation, for instance, where positive and negative solutions are related to two different kinds of fermionic particles: electrons and positrons, respectively.

In a superconducting system, however, there is additionally a similar *pseudo-reality* constraint on the fermion field operator  $\Psi$ ,

$$C_{jk} \Psi_k^\dagger = \Psi_j \quad (1.21)$$

(summation over the index  $k$  is implied), which yields anti-commutation relations of Majorana form:

$$\{\Psi_j(\vec{r}), \Psi_k(\vec{r}')\} = C_{jk} \delta(\vec{r} - \vec{r}') \quad (1.22)$$

$$\{\Psi_j(\vec{r}), \Psi_k^\dagger(\vec{r}')\} = \delta_{jk} \delta(\vec{r} - \vec{r}') . \quad (1.23)$$

These symmetry properties are a necessary consequence of the redundancy inherent to the Nambu formalism for superconductors, which causes the physical excitations to be represented twice in the spectrum: the creation of a quasi-particle with positive energy is *identical* to the annihilation of the corresponding negative-energy state.

The conditions in Eqs. (1.19) and (1.21) are sufficient to prove that, by unitary transformation, the Hamiltonian can be brought to a purely imaginary form, with all eigenmodes—not just those at zero energy—having a representation as real, Majorana-like fields [12].

# 2

## Chapter 2

---

# Jordan–Wigner transformations for tree structures

*The Jordan–Wigner transformation provides an efficient spin–fermion mapping in one-dimensional systems (cf. Sec. 1.1). An extension of this mapping, which relates fermionic and spin- $\frac{1}{2}$  systems with nearest-neighbour coupling, to arbitrary tree structures is presented in the following. This generalised Jordan–Wigner transformation is made possible with the help of additional spins at the junctions between one-dimensional chains. The extended mapping allows for straightforward simulations of Majorana braiding in spin or qubit systems. The results contained in this chapter have been published in Ref. [14].*

## 2.1 Spin–fermion mapping beyond 1D

As the Jordan–Wigner transformation (Sec. 1.1) provides a locality-preserving mapping between chains of spins and of fermions, it is very useful in *one-dimensional* systems. However, a naive application to higher-dimensional systems generally results in a strong non-locality: The transformation requires imposing a 1D order to construct the string operators used to relate the commuting operators of different spins to anti-commuting fermion operators. In a system which is not strictly one-dimensional, these string operators do not cancel each other for all kinds of local terms in the Hamiltonian.

There are some more sophisticated approaches to higher-dimensional systems: One method is the use of a multi-dimensional phase factor instead of the one-dimensional string. In this case, the transformation creates a fictitious gauge field [15] and may result in the attachment of flux tubes to the system operators [16]. In a different approach, additional degrees of freedom are introduced to cancel the strings, which means that the transformation yields a local, yet more complicated Hamiltonian and the original properties of the system are preserved in the low-energy sector only [17].

A simpler modification of the Jordan–Wigner transformation was proposed for a more particular system geometry: Without relinquishing locality, a three-leg star graph of free fermions can be mapped to quadratic spin chains connected via specific 3-spin couplings [18]. Furthermore, Ref. [18] describes a locality-preserving mapping of quadratic three-leg spin graphs with XY coupling to a Kondo-like system of fermionic chains coupled by one spin. In this chapter, we will demonstrate that both transformations can be generalised to tree structures of one-dimensional chains.

This kind of transformation can, e.g., be used to obtain a spin representation for the braiding

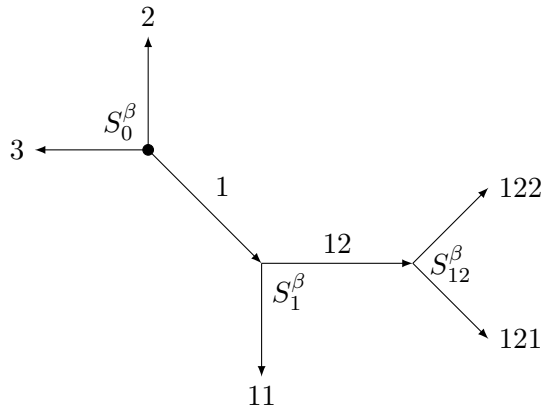


**Figure 2.1:** Binary-tree structure consisting of fermionic or spin chains. In each chain, spins or fermions are numbered in arrow direction. The chains themselves are identified by sequential numbers that are appended to the label of their parent chain (if there is one). The root is the only vertex that has no incoming edge and may have three outgoing edges. At the inner vertices, there are additional spins with Pauli matrices  $S_\alpha^\beta$  ( $\alpha = 0$  at the root, the label of the ingoing chain elsewhere).

of fermionic Majorana modes (cf. Sec. 1.4) in a T-junction geometry. For both the case of a single topological interval and Majorana modes from two topological intervals, an explicit description of a Majorana braiding operation translated into the corresponding spin system is given in App. A.

## 2.2 Geometry and notations

A priori, the tree structures we consider do not have directions or a distinctive root. For the purposes of the transformation, however, we have to choose an arbitrary vertex as root and assign each edge (i. e. chain) an orientation away from it. To reflect this hierarchy, the outgoing chains of a vertex are denoted by sequential numbers that are, if applicable, appended to the label of their parent chain (ingoing chain of the vertex).

According to the orientation, the spins or fermions in a chain  $\alpha$  are numbered from 1 to  $L_\alpha$ ; they are represented by the Pauli matrices  $\sigma_\alpha^\beta(j)$  and the fermionic creation/annihilation operators  $c_\alpha^\dagger(j)/c_\alpha(j)$ , respectively. Pauli matrices  $S_\alpha^\beta$  represent additional spins located at the inner vertices that are required for the transformations; here  $\alpha$  is the label of the ingoing chain (or  $\alpha = 0$  at the root). An example of a permissible tree structure is depicted in Fig. 2.1.

We use separate Jordan–Wigner transformations for each chain  $\alpha$ ,

$$c_\alpha(j) = \eta_\alpha \left[ \prod_{k=1}^{j-1} \sigma_\alpha^z(k) \right] \sigma_\alpha^-(j) \quad (2.1a)$$

$$c_\alpha^\dagger(j) = \eta_\alpha \left[ \prod_{k=1}^{j-1} \sigma_\alpha^z(k) \right] \sigma_\alpha^+(j) , \quad (2.1b)$$

with  $\sigma_\alpha^\pm(j) = \frac{1}{2} [\sigma_\alpha^x(j) \pm i \sigma_\alpha^y(j)]$ . The factors  $\eta_\alpha$  with  $\eta_\alpha^2 = 1$  have to be chosen in such a way that

proper (anti-)commutation relations between operators of different chains result. The relation

$$\sigma_\alpha^z(j) = 2c_\alpha^\dagger(j)c_\alpha(j) - 1 = 1 - 2c_\alpha(j)c_\alpha^\dagger(j) \quad (2.2)$$

is a useful corollary of these definitions. Hence, a (magnetic) field acting in  $z$  direction on a spin corresponds to a local chemical potential at a fermionic site.

## 2.3 Free fermions and 3-spin couplings

To complete the description of the transformation, we need to define the operators  $\eta_\alpha$ . For the chains directly at the root,  $\alpha \in \{1, 2, 3\}$ , the definition of the transformation in Ref. [18] is used:

$$\eta_\alpha = S_0^\alpha . \quad (2.3a)$$

For all the other chains, denoted by  $\alpha\beta$  with parent chain  $\alpha$  and  $\beta \in \{1, 2\}$ , we define:

$$\eta_{\alpha\beta} = \eta_\alpha \left[ \prod_{k=1}^{L_\alpha} \sigma_\alpha^z(k) \right] S_\alpha^\beta . \quad (2.3b)$$

These definitions satisfy the conditions stated in the previous section.

Within a one-dimensional chain, the Jordan–Wigner transformation is known to convert local quadratic fermionic Hamiltonians into local quadratic spin Hamiltonians (Sec. 1.1); the factors  $\eta_\alpha^2 = 1$  in Eqs. (2.1) do not affect this. Therefore we will examine only the couplings at the vertices between different chains. There are two kinds of vertex couplings: those between a parent and a descendant chain and those between two descendant chains of the same parent. A coupling term of the first kind between chains  $\alpha$  and  $\alpha\beta$ , with  $\beta \in \{1, 2\}$ , has the general form

$$H_{\alpha\beta} = u c_\alpha(L_\alpha) c_{\alpha\beta}(1) + t c_\alpha^\dagger(L_\alpha) c_{\alpha\beta}(1) + \text{H. c.} , \quad (2.4a)$$

which is transformed, using the relation (2.1), into

$$H_{\alpha\beta}^S = S_\alpha^\beta \left[ u \sigma_\alpha^-(L_\alpha) \sigma_{\alpha\beta}^-(1) - t \sigma_\alpha^+(L_\alpha) \sigma_{\alpha\beta}^-(1) + \text{H. c.} \right] . \quad (2.4b)$$

A coupling of the second kind between chains  $\alpha\beta$  and  $\alpha\gamma$  (here  $\beta, \gamma \in \{1, 2\}$ ,  $\beta \neq \gamma$ ; at the root,  $\alpha$  is empty and  $\beta, \gamma \in \{1, 2, 3\}$ ,  $\beta \neq \gamma$ ) has the general form

$$H_{\alpha(\beta,\gamma)} = u c_{\alpha\beta}(1) c_{\alpha\gamma}(1) + t c_{\alpha\beta}^\dagger(1) c_{\alpha\gamma}(1) + \text{H. c.} , \quad (2.5a)$$

which is similarly mapped to

$$\begin{aligned} H_{\alpha(\beta,\gamma)}^S &= S_\alpha^\beta S_\alpha^\gamma \left[ u \sigma_{\alpha\beta}^-(1) \sigma_{\alpha\gamma}^-(1) + t \sigma_{\alpha\beta}^+(1) \sigma_{\alpha\gamma}^-(1) \right] + \text{H. c.} \\ &= S_\alpha^\nu \epsilon_{\beta\gamma\nu} \left[ i u \sigma_{\alpha\beta}^-(1) \sigma_{\alpha\gamma}^-(1) + i t \sigma_{\alpha\beta}^+(1) \sigma_{\alpha\gamma}^-(1) + \text{H. c.} \right] , \end{aligned} \quad (2.5b)$$

where  $\epsilon_{\beta\gamma\nu}$  is the Levi-Civita symbol.

This transformation can be generalised, beyond binary trees, to arbitrary tree structures: Any higher-order vertex (with more than three edges) can be thought of as built out of multiple three-edge vertices, connected by chains of length zero. For instance, the structure depicted in Fig. 2.1 can be viewed as a five-edge vertex; the zero-length internal chains (1 and 12) do not contribute products to the Klein factors, in this case, but coupling terms involving more than three spins may appear.

## 2.4 XY spin system and fermionic Kondo model

In this section, we consider a tree structure of spins with local XY couplings and use the Jordan–Wigner transformation to obtain the corresponding fermionic Hamiltonian. A single one-dimensional XY spin chain is simply mapped to free fermions (cf. Sec. 1.1). The generalised transformation defined in Eqs. (2.1) and (2.3), however, involves additional spin operators  $S_\alpha^\beta$ , which can either commute with the spins or with the fermion operators in the chains, but not both.

To simplify the resulting fermionic Hamiltonian, we introduce new spin operators  $\tilde{S}_\alpha^\beta$  at the inner vertices. These operators do not appear in the spin Hamiltonian, and they commute with all the spins in the chains. Concerning the spin operators  $S_\alpha^\beta$  appearing in the transformation (2.1), we need to take special care of their commutation relations with the fermionic operators. Therefore we define

$$S_0^\beta = \tilde{S}_0^\beta \prod_{\substack{\text{chain labels } \gamma \\ \text{not beginning} \\ \text{with } \beta}} P_\gamma \quad \text{and} \quad S_\alpha^\beta = \tilde{S}_\alpha^\beta \prod_{\substack{\text{chain labels } \alpha\gamma \\ \text{not beginning} \\ \text{with } \alpha\beta}} P_{\alpha\gamma}, \quad (2.6)$$

using the abbreviated notation

$$P_\alpha = \left[ \prod_{k=1}^{L_\alpha} \sigma_\alpha^z(k) \right] \quad (2.7)$$

for the fermionic parity of chain  $\alpha$ . As the products consist of Pauli matrices  $\sigma^z$  only, operators  $S_\alpha^\beta$  inherit the commutation relations of  $\tilde{S}_\alpha^\beta$ . Therefore  $S_\alpha^\beta$  are spin- $\frac{1}{2}$  operators, which can most easily be seen by example. We can specify them, e. g., for the tree structure depicted in Fig. 2.1:

$$S_0^1 = \tilde{S}_0^1 P_2 P_3 \quad (2.8a)$$

$$S_0^2 = \tilde{S}_0^2 \left[ P_1 P_{11} (P_{12} P_{121} P_{122}) \right] P_3 \quad (2.8b)$$

$$S_0^3 = \tilde{S}_0^3 \left[ P_1 P_{11} (P_{12} P_{121} P_{122}) \right] P_2 \quad (2.8c)$$

(the grouping highlights the tree structure),

$$S_1^1 = \tilde{S}_1^1 (P_{12} P_{121} P_{122}) \quad (2.9a)$$

$$S_1^2 = \tilde{S}_1^2 P_{11} \quad (2.9b)$$

$$S_1^3 = \tilde{S}_1^3 P_{11} (P_{12} P_{121} P_{122}) \quad (2.9c)$$

and

$$S_{12}^1 = \tilde{S}_{12}^1 P_{122} \quad (2.10a)$$

$$S_{12}^2 = \tilde{S}_{12}^2 P_{121} \quad (2.10b)$$

$$S_{12}^3 = \tilde{S}_{12}^3 P_{121} P_{122} . \quad (2.10c)$$

The parity operators, i. e. products of  $\sigma^z$  across one chain, guarantee that  $S_\alpha^\beta$  commute with the fermionic operators of all chains.

Again, the Jordan–Wigner transformation is known to map XY-coupled spins in a 1D chain to free fermions, so we only have to examine the two kinds of vertex couplings, as we did in the preceding

section. They result in Kondo-like couplings of the fermionic chains:

$$H_{\alpha\beta} = u \sigma_{\alpha}^{-}(L_{\alpha}) \sigma_{\alpha\beta}^{-}(1) + t \sigma_{\alpha}^{+}(L_{\alpha}) \sigma_{\alpha\beta}^{-}(1) + \text{H. c.} \quad (2.11a)$$

$$\longrightarrow H_{\alpha\beta}^{\text{F}} = S_{\alpha}^{\beta} \left[ u c_{\alpha}(L_{\alpha}) c_{\alpha\beta}(1) - t c_{\alpha}^{\dagger}(L_{\alpha}) c_{\alpha\beta}(1) + \text{H. c.} \right] \quad (2.11b)$$

and

$$H_{\alpha(\beta,\gamma)} = u \sigma_{\alpha\beta}^{-}(1) \sigma_{\alpha\gamma}^{-}(1) + t \sigma_{\alpha\beta}^{+}(1) \sigma_{\alpha\gamma}^{-}(1) + \text{H. c.} \quad (2.12a)$$

$$\begin{aligned} \longrightarrow H_{\alpha(\beta,\gamma)}^{\text{F}} &= S_{\alpha}^{\beta} S_{\alpha}^{\gamma} \left[ u c_{\alpha\beta}(1) c_{\alpha\gamma}(1) + t c_{\alpha\beta}^{\dagger}(1) c_{\alpha\gamma}(1) \right] + \text{H. c.} \\ &= S_{\alpha}^{\nu} \epsilon_{\beta\gamma\nu} \left[ i u c_{\alpha\beta}(1) c_{\alpha\gamma}(1) + i t c_{\alpha\beta}^{\dagger}(1) c_{\alpha\gamma}(1) + \text{H. c.} \right]. \end{aligned} \quad (2.12b)$$

Thus, inter-chain couplings are mediated by the spin at the corresponding vertex.

## 2.5 Majorana braiding and the spin representation

Majorana modes arising in the topological phase of the Kitaev chain (Sec. 1.3), a one-dimensional fermionic system, can be braided in a T-junction geometry by local tuning of the chemical potential (cf. Sec. 1.4). The modified Jordan–Wigner transformation described in Ref. [18] and Sec. 2.3 provides us with a spin representation of this free-fermion system. In the following, the spin indices are swapped in such a way that the resulting Ising couplings are in the  $z$  component and transverse fields in the  $x$  direction. Furthermore, we use fermionic Majorana operators  $\gamma_{\alpha}(m)$ , as defined in Sec. 1.2, to express the transformation in a convenient form:

$$\gamma_{\alpha}(2j-1) = \eta_{\alpha} \left[ \prod_{k=1}^{j-1} \sigma_{\alpha}^x(k) \right] \sigma_{\alpha}^z(j) \quad (2.13a)$$

$$\gamma_{\alpha}(2j) = \eta_{\alpha} \left[ \prod_{k=1}^{j-1} \sigma_{\alpha}^x(k) \right] \sigma_{\alpha}^y(j) \quad (2.13b)$$

$$\Rightarrow \sigma_{\alpha}^x(j) = i \gamma_{\alpha}(2j-1) \gamma_{\alpha}(2j). \quad (2.14)$$

The Klein factors  $\eta_{\alpha}$  are those defined in Eqs. (2.3).

The transformation relates the topological (nontopological) phase in the fermionic chains to the ferromagnetic (paramagnetic) phase of the spin system (for more details see App. A.1). Now we can simply translate into the spin system the unitary operator produced by, e. g., counter-clockwise braiding of Majorana modes  $\gamma_A, \gamma_B$  (cf. Sec. 1.4):

$$U = \exp\left(-\frac{\pi}{4} \gamma_A \gamma_B\right). \quad (2.15)$$

In the case of two Majorana modes provided by one topological interval, which is located on a single chain before and after the braiding, the Klein factors cancel in the spin representation, so the additional spin mediating the coupling at the junction does not influence the result of the operation and is left unaffected at the end (see Apps. A.2 and A.3).

Braiding neighbouring Majorana modes from two topological intervals on different chains corresponds to a more complicated operation in the spin system. By choosing, e. g.,  $\gamma_A = \gamma_1(2m-1)$  from the first

chain and  $\gamma_B = \gamma_3(2n - 1)$  from the third chain, we obtain:

$$\begin{aligned}
 U_{1,3} &= \exp \left[ -\frac{\pi}{4} \cdot S_0^x \prod_{j=1}^{m-1} \sigma_1^x(j) \cdot \sigma_1^z(m) \cdot S_0^z \prod_{k=1}^{n-1} \sigma_3^x(k) \cdot \sigma_3^z(n) \right] \\
 &= \exp \left[ i \frac{\pi}{4} S_0^y \cdot \sigma_1^z(m) \prod_{j=1}^{m-1} \sigma_1^x(j) \prod_{k=1}^{n-1} \sigma_3^x(k) \cdot \sigma_3^z(n) \right] \\
 &\xrightarrow{\text{effectively}} \exp \left[ i \frac{\pi}{4} S_0^y \sigma_1^z(m) \sigma_3^z(n) \right] , \tag{2.16}
 \end{aligned}$$

if the spins outside the ferromagnetic intervals are polarised in  $x$  direction. A detailed description of this operation in the spin language is given in App. A.4.

The spin equivalent of braiding Majorana operators further away from each other involves, consequently, the additional spins at all the intermediate vertices. For  $\gamma_A = \gamma_{12}(2m - 1)$  and  $\gamma_B = \gamma_3(2n - 1)$ , e. g., this yields:

$$\begin{aligned}
 U_{12,3} &= \exp \left[ -\frac{\pi}{4} \cdot S_0^x \prod_{j=1}^{L_1} \sigma_1^x(j) \cdot S_1^y \prod_{k=1}^{m-1} \sigma_{12}^x(k) \cdot \sigma_{12}^z(m) \cdot S_0^z \prod_{l=1}^{n-1} \sigma_3^x(l) \cdot \sigma_3^z(n) \right] \\
 &= \exp \left[ i \frac{\pi}{4} S_0^y S_1^y \cdot \sigma_{12}^z(m) \prod_{k=1}^{m-1} \sigma_{12}^x(k) \prod_{j=1}^{L_1} \sigma_1^x(j) \prod_{l=1}^{n-1} \sigma_3^x(l) \cdot \sigma_3^z(n) \right] . \tag{2.17}
 \end{aligned}$$

This expression contains a string of all the spin operators that are needed to connect the two original sites in the tree structure (Fig. 2.1). From a quantum-information perspective, this is a complex operation, which involves a multitude of spins (qubits) and, in general, entangles the spins in the chains with the additional spins at vertices. On the other hand, this complexity and entanglement can be seen as a crucial property for the simulation of *fermionic quantum computation* in a bosonic system.

## 2.6 Conclusion

In general, Jordan–Wigner transformations provide a *locality-preserving* mapping between Hamiltonians of spins and of fermions in strictly one-dimensional systems only. However, the scope of this property can be extended significantly by introducing additional spins at three-chain junctions, as it was described for the special case of a star graph before [18]. In this chapter, we have shown that the same method can, in fact, be used for binary-tree structures. Thereby, fermionic trees are mapped to spin trees with particular 3-spin couplings at the vertices, and XY spin trees are mapped to fermionic trees with Kondo-like couplings between the chains. This transformation provides, e. g., a spin equivalent of Majorana braiding operations. We have further shown that this construction can be generalised to arbitrary tree structures.

It must be noted that these mappings involve an enlargement of the original Hilbert space: in the case of XY spins due to the addition of spins  $\tilde{S}_\alpha$  to the system, in the case of free fermions implicitly during the transformation. Thus, the degeneracy of all states is multiplied by a factor of 2 to the power of the number of inner vertices, but the accuracy of the mapping is not affected.

# 3

## Chapter 3

# Current correlation in a Majorana system with charging energy

*In a regular superconductor, the tunneling of single electrons into and out of the system is energetically disfavoured due to the pairing gap. Majorana zero modes in a topological superconductor (cf. Sec. 1.3), on the other hand, enable gapless tunneling of unpaired electrons. Despite their non-local nature, two spatially separate Majorana modes cannot by themselves mediate current correlations between different contacts tunnel-coupled to the system. In the presence of Coulomb interactions, however, the charging energy causes correlations between tunnel currents. For the regime of a small charging energy, these current correlations are calculated in the following.*

## 3.1 Transport through Majorana modes

Besides their potential use for quantum computation (cf. Sec. 1.4), Majorana zero modes in topological superconductors have also been studied in transport settings (see e.g. References [19–24]). In a *grounded* Majorana system, contacts at perfect, non-overlapping zero modes show ideal Andreev reflection without any correlation between the currents mediated by different Majorana modes [19].

A large charging energy in the regime of strong *Coulomb blockade*, on the other hand, effects a coherent transport (“teleportation”) of single electrons between the contacts at two Majorana zero modes [21]; in this case, both tunneling currents are perfectly correlated. In between these two extreme cases, the onset of correlations in the limit of small charging energy is analysed in this chapter.

## 3.2 Model

We consider a mesoscopic topologically superconducting wire (island) hosting two Majorana zero modes at the ends (cf. the toy model in Sec. 1.3), which are contacted by a left and a right normal-conducting lead. In deriving an effective *Keldysh* action in terms of the phase  $\phi$  of the island, we generally follow the approach in Ref. [22] (cf. App. B.1): The superconducting gap  $\Delta$  is assumed to be sufficiently larger than other energy scales involved that transport is mediated by the zero modes only and no higher-energy quasi-particles are relevant. The effective action consists of two contributions, resulting from the charging energy and the fermionic dynamics, respectively:

$$iS = iS_c + iS_f . \quad (3.1)$$

The first contribution is due to charging energy  $E_c$  on the island and has the form:

$$iS_c = i \int dt \dot{\phi}_q \left( \frac{\dot{\phi}_c}{2E_c} + n_0 \right). \quad (3.2)$$

The dependence on the gate charge  $q_0 = n_0 e$  will not be relevant in the regime of small charging energy  $E_c$ . In order to obtain the second, fermionic contribution, the normal-conducting leads are integrated out in a wide-band approximation; subsequent integration over the Majorana fermion fields and expansion up to the second power in the quantum Keldysh component  $\phi_q$  yields

$$iS_f = i \int dt \mathcal{I}(t) \phi_q(t) - \frac{1}{2} \int dt dt' \phi_q(t) K(t-t') \phi_q(t') + \mathcal{O}(\phi_q^3). \quad (3.3)$$

Both the fluctuation kernel  $K(t-t') = \sum_j K_j(t-t')$ , see App. B.2, and the operator of the current flowing into the dot  $\mathcal{I}(t) = \sum_j \mathcal{I}_j(t)$  can be separated into contributions from the left and right contact,  $j \in \{L, R\}$ . The current operators are given by

$$\mathcal{I}_j(t) = \Gamma_j \int dt' F(t'-t) \sin \Phi_j(t', t) G_j^R(t-t'), \quad (3.4)$$

with Majorana Green's functions

$$G_j^R(t) = -i \Theta(t) e^{-\Gamma_j t} \iff G_j^R(\omega) = \frac{1}{\omega + i\Gamma_j} \quad (3.5)$$

broadened by the coupling to the relevant lead. The (equilibrium) distribution function  $F$  applies to both leads, as the chemical potentials are included in the quantity

$$\Phi_j(t, t') = V_j(t-t') + \phi_c(t) - \phi_c(t') \quad (3.6)$$

depending on the voltage  $V_j$  at the relevant contact and the classic Keldysh component  $\phi_c$ . (Adjustment of the chemical potential of the island distributes the total voltage between the left and right lead in such a way that a steady state with vanishing total current  $\mathcal{I}$  emerges.)

### 3.3 Langevin equation

In order to describe the currents at both contacts and their (correlated) fluctuations, it is useful to decouple the  $\phi_q$ -quadratic terms of the action by means of two separate Hubbard–Stratonovich transformations. Thereby we introduce two noise fields  $\xi_L, \xi_R$  (see also App. B.2):

$$\begin{aligned} & \prod_j \exp \left[ -\frac{1}{2} \int dt dt' \phi_q(t) K_j(t-t') \phi_q(t') \right] \\ &= \int D[\xi_L, \xi_R] \prod_j \exp \left[ -\frac{1}{2} \int dt dt' \xi_j(t) K_j^{-1}(t-t') \xi_j(t') + i \int dt \phi_q(t) \xi_j(t) \right]. \end{aligned} \quad (3.7)$$

The two fields are uncorrelated and their Gaussian noise averages are determined by their fluctuation kernels  $K_j$ ,

$$\langle \xi_j(t) \xi_k(t') \rangle = \delta_{jk} K_j(t-t'). \quad (3.8)$$

The evaluation of the action is facilitated by expanding it in the classical Keldysh component of the phase, too. Approximation of  $\mathcal{I}(t)$  to first order in  $\phi_c$  and integration over  $\phi_q$  leads to a Langevin equation for the classical phase:

$$\frac{1}{2E_c} \ddot{\phi}_c + \int^t dt' \eta(t-t') \dot{\phi}_c(t') = \sum_j \xi_j(t). \quad (3.9)$$

Here, the sum of noise fields corresponds to the single noise field  $\xi$  in the calculation of Ref. [22]. Using the retarded Greens' function (propagator)  $D^R$  of this equation, we can express the phase

$$\bar{\phi}_c(t) = \int d\tau D^R(t-\tau) \sum_j \xi_j(\tau) \quad (3.10)$$

as a function of the fluctuation fields  $\xi_j$ . Further approximations in the low-energy limit and the evaluation of noise averages are described in App. B.3.

### 3.4 Currents and correlations

To determine the expressions for the currents and their correlations, we carry out a variational calculation in the relevant counting fields at first, using the counting-field-dependent part of the action (cf. App. B.2)

$$iS_\xi[\chi_L, \chi_R] = i \sum_j \int dt [\mathcal{I}_j(t) + \xi_j(t)] [\phi_q(t) + \chi_j(t)] - \frac{1}{2} \sum_j \int dt dt' \xi_j(t) K_j^{-1}(t-t') \xi_j(t'). \quad (3.11)$$

Then, we set the counting fields to zero and integrate out  $\phi_q$ , which leads to the Langevin equation (3.9) for the classical phase. The solution (3.10) gives  $\bar{\phi}_c$  as a function of the fluctuation fields  $\xi_j$ , which remain as the only fields of the path integral.

The operator for the current at contact  $j$  can be calculated by performing a single variation of the action  $S_\xi$  in the counting field  $\chi_j$ ,

$$\frac{\delta S_\xi[\chi_L, \chi_R]}{\delta \chi_j(t)} = \mathcal{I}_j(t) + \xi_j(t), \quad (3.12)$$

so the current is given by

$$I_j(t) = \langle \mathcal{I}_j(t) + \xi_j(t) \rangle_\xi = \langle \mathcal{I}_j(t) \rangle_\xi. \quad (3.13)$$

In order to calculate the correlation between left and right current, we need to vary the action in both counting fields. Thereby we obtain the expression

$$C_{LR}(t_L - t_R) = \left\langle \left[ \mathcal{I}_L(t_L) + \xi_L(t_L) \right] \left[ \mathcal{I}_R(t_R) + \xi_R(t_R) \right] \right\rangle_\xi - I_L(t_L) I_R(t_R). \quad (3.14)$$

While the fluctuation fields  $\xi_L, \xi_R$  are uncorrelated, they both appear in the classical phase  $\bar{\phi}_c$ . Hence, we have to consider multiple terms for the correlation:

$$C_{LR}(t_L - t_R) = \left\langle \mathcal{I}_L(t_L) \xi_R(t_R) + \xi_L(t_L) \mathcal{I}_R(t_R) \right\rangle_\xi + \left\langle \mathcal{I}_L(t_L) \mathcal{I}_R(t_R) \right\rangle_\xi - I_L(t_L) I_R(t_R). \quad (3.15)$$

For completeness, the autocorrelation of the current at contact  $j$  is given by the expression

$$C_{jj}(t_1 - t_2) = K_j(t_1 - t_2) + \left\langle \mathcal{I}_j(t_1) \xi_j(t_2) + \xi_j(t_1) \mathcal{I}_j(t_2) \right\rangle_\xi + \left\langle \mathcal{I}_j(t_1) \mathcal{I}_j(t_2) \right\rangle_\xi - I_j(t_1) I_j(t_2) , \quad (3.16)$$

which additionally contains  $K_j$  itself, yielding a finite expectation value even without charging energy.

### 3.5 Low-energy limit

In addition to a small charging energy  $E_c = \Omega/\eta_0 \sim \Omega$  (with  $\eta_0 \approx \frac{4}{\pi}$ , cf. App. B.3), we assume small voltages as well as a small temperature, compared to the tunnel couplings  $\Gamma_j$ , and we focus on low energies, i. e.

$$\Gamma_j \gg \Omega, |V_j|, T, |\omega| \sim |t_L - t_R|^{-1} . \quad (3.17)$$

In this limit, the symmetrised correlation  $C = \frac{1}{2}(C_{LR} + C_{RL})$  is approximately given by (see App. C.1)

$$C(\omega) \approx -\frac{3}{16} \frac{\Omega^2}{\omega^2 + \Omega^2} K(\omega) . \quad (3.18)$$

The dependence of the prefactor on the charging energy  $\Omega$  affects the width of the spectrum. This  $\Omega$ -dependent factor can also be written as  $\Omega \cdot \delta_\Omega(\omega)$ , where  $\delta_\Omega$  is the approximation of the  $\delta$  function with width  $\Omega$ .

We can express the fluctuation kernel  $K = K_L + K_R$  analytically for two different regimes: In equilibrium ( $V_j = 0$ ),  $K$  is determined via a fluctuation–dissipation relation [22], which yields the low-frequency expressions

$$K_j^{\text{eq}}(\omega) \approx \frac{\eta_0 \omega}{4} \coth\left(\frac{\omega}{2T}\right) . \quad (3.19)$$

Hence, the correlation function  $C$  takes on the form

$$C_{\text{eq}}(\omega) \approx -\frac{3}{8\pi} \frac{\Omega^2}{\omega^2 + \Omega^2} \omega \coth\left(\frac{\omega}{2T}\right) . \quad (3.20)$$

The zero-frequency correlation value depends on the temperature  $T$  in this case.

At  $T = 0$ , on the other hand, the fluctuation kernels  $K_j(\omega) \approx K_j^0(\omega) + K_j^V(\omega)$  comprise two different terms (cf. App. C.2): The first one is approximately given by a linear spectrum, which yields the correlation expression

$$C_0(\omega) \approx -\frac{3}{8} \frac{\Omega^2}{\omega^2 + \Omega^2} |\omega| . \quad (3.21)$$

At small frequencies  $|\omega| \lesssim |V_k^3|/\Gamma_k^2$ , the voltage-dependent terms  $K_j^V$  can be relevant:

$$\Rightarrow C_V(\omega) \approx -\frac{1}{8\pi} \frac{\Omega^2}{\omega^2 + \Omega^2} \sum_k \left( \frac{|V_k^3|}{\Gamma_k^2} - \frac{3V_k^2}{2\Gamma_k^2} |\omega| \right) , \quad |\omega| \ll |V_k| . \quad (3.22)$$

If the voltages are vanishingly small, e. g.  $|V_k| \lesssim \Omega^3/\Gamma_k^2$  in the symmetric case  $\Gamma_L = \Gamma_R$ , the zero-frequency correlation is determined by an additional contribution instead, which yields the value (cf. App. C.2)

$$C_\Omega(\omega) \approx \frac{V_L V_R \Omega^3}{32 \Gamma_L^2 \Gamma_R^2} \frac{\Omega^2}{\omega^2 + 4 \Omega^2}, \quad |\omega| \ll \Omega. \quad (3.23)$$

Note that  $V_L$  and  $V_R$  have opposite signs in the steady state, so the correlation at  $\omega = 0$  is always negative.

## 3.6 Conclusion

Majorana zero modes in a topological superconductor can mediate the tunneling of single electrons to normal-conducting leads. But in a system without charging energy, tunnel currents at two perfect zero modes coupled to two separate contacts are uncorrelated. Although a small charging energy does not have much impact on the individual currents, it causes correlations between the current fluctuations. For a low-energy regime, the correlated fluctuations have been analysed in this chapter.

In the equilibrium (zero-voltage) case, a fluctuation–dissipation relation facilitates obtaining a temperature-dependent expression for the symmetrised correlation function. We have also derived analytical approximations for the correlation in the finite-voltage, zero-temperature limit. Interestingly, for finite temperatures or voltages, the charging-energy scale  $\Omega$  does not significantly affect the zero-frequency value of the correlation. As the correlation function decays proportional to  $1/\omega^2$  for larger frequencies  $\omega$ , however,  $\Omega$  acts as a characteristic energy scale for the width of the correlation spectrum in both cases.



# 4

## Current–phase relation in a long topological Josephson junction

*The surface of a three-dimensional topological insulator (TI) can be gapped out by proximity coupling to a ferromagnet or a superconductor. Boundaries between differently gapped regions support one-dimensional gapless states, among them Majorana modes (cf. Sec. 1.5). This chapter discusses a long Josephson junction formed by two s-wave superconductors on a TI surface, with either a ferromagnetic or an ungapped region in the middle. Generally, the Josephson current mediated by the TI surface is determined by scattering modes as well as by the states localised around the junction. This analysis of the current–phase relation in a topological Josephson junction takes into account both contributions.*

### 4.1 Proximity effects on a topological insulator

Proximity effects of superconductors and ferromagnets on the surface of a strong topological insulator were predicted to permit the realisation of both zero-dimensional and one-dimensional Majorana modes (Sec. 1.5) by Fu and Kane [3]. Several works have since analysed the properties of topological Josephson junctions on a TI surface: For the case of a ferromagnetic insulator separating the superconductors (SMS geometry), the Josephson current resulting from Andreev *bound states*, in the form of chiral Majorana modes, has been calculated for s-wave superconductors [25] and for different superconducting pairings [26]; both a ferromagnetic and an ungapped middle region (SNS case) were considered in Ref. [27]. Recently, a Josephson Hall current, perpendicular to the regular Josephson current, was derived from *scattering-state* wave functions in a SMS system [28].

Theoretical analysis so far has focused on the—experimentally most relevant—case of a large chemical potential  $\mu$  in comparison to the superconducting gap on the TI surface. In the limit  $\mu = 0$ , the current carried by chiral Dirac modes between the chiral Majorana modes of a topological Josephson junction was evaluated in Ref. [29], but the Josephson current in a plain, translation-invariant SMS or SNS geometry has not been calculated so far. In the following, such a Josephson junction will be analysed in the—presently at least theoretically—interesting limit of a vanishing chemical potential.

### 4.2 Electronic modes

On the surface of a topological insulator, two regions gapped by superconductors surrounding an either ungapped or ferromagnetically gapped stripe form a Josephson junction (Fig. 4.1). For simplicity, we

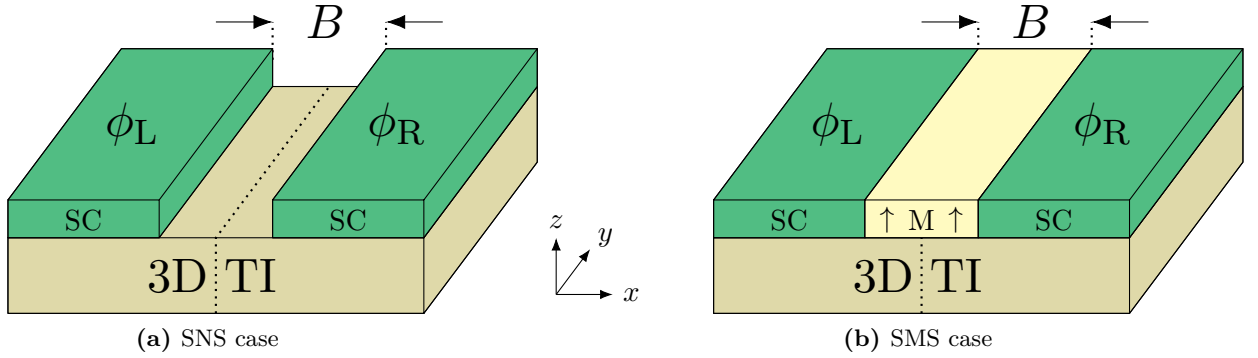


**Figure 4.1:** Two s-wave superconductors (SC) with phases  $\phi_L$ ,  $\phi_R$  form a long Josephson junction of width  $B$  on the surface of a three-dimensional topological insulator (3D TI). In the middle, the TI surface either remains ungapped (a), or it is gapped by a ferromagnetic insulator (M) with magnetisation perpendicular to the surface (b). The dotted lines on the TI mark the intersection with the plane  $x = 0$ .

assume that the system is homogenous along the  $y$  direction. The Hamiltonian for the surface states (cf. Sec. 1.5) is given by

$$H = E_O + \frac{1}{2} \int dx dy \Psi^\dagger h \Psi, \quad (4.1a)$$

$$h = v \vec{p} \cdot \vec{\sigma} \tau_z + M(x) \sigma_z + \Delta(x) \tau_- + \Delta^*(x) \tau_+, \quad (4.1b)$$

with an energy offset  $E_O$ , the fermion fields  $\Psi = [\psi_\uparrow, \psi_\downarrow, \psi_\downarrow^\dagger, -\psi_\uparrow^\dagger]^\top$ , the Fermi velocity  $v > 0$  and the 2D momentum operator  $\vec{p} = -i \hbar \nabla$ . Pauli matrices  $\sigma_j$  and  $\tau_j$  act in spin and Nambu space, respectively. We consider the superconducting order parameter to be of the same magnitude  $\Delta_0 > 0$  on both sides,

$$\Delta(x) = \Delta_0 \left[ \Theta(-x - B/2) e^{i\phi_L} + \Theta(x - B/2) e^{i\phi_R} \right], \quad (4.2)$$

where  $B > 0$  and  $\Theta$  is the Heaviside function, and analyse the system for a magnetic gap

$$M(x) = M_0 \Theta(B/2 - |x|) \quad (4.3)$$

in the limits of  $M_0 = 0$  and  $M_0 = \Delta_0$ , with an arbitrary phase difference  $\chi = \phi_L - \phi_R$ .

The eigenmodes of  $h$  can be assembled from the piecewise solutions in the three different regions. Due to translation invariance, the  $y$  dependence of all modes is given by plain waves  $\exp(iqy/\hbar)$  with momentum  $q$ . In contrast, the solutions generally involve different momenta  $k$  along the  $x$  axis, including imaginary values of  $k$  for states that are localised in  $x$  direction around the junction. As negative-energy modes  $\xi_- = \sigma_y \tau_y \xi_+^*$  are just the particle-hole inverted doublets of positive-energy solutions  $\xi_+$ , it is sufficient only to consider energies  $\epsilon > 0$  in the following. In the central region, we can distinguish electron modes,

$$\xi_{kMq}^{(e)}(x, y) = \frac{1}{\sqrt{(\epsilon_M - M_0)^2 + v^2 |k_M + iq|^2}} \begin{bmatrix} \epsilon_M - M_0 \\ v(k_M + iq) \\ 0 \\ 0 \end{bmatrix} e^{ik_M x/\hbar} e^{iqy/\hbar}, \quad (4.4a)$$

and hole modes of the same energy  $\epsilon_M = \sqrt{M_0^2 + v^2 (k_M^2 + q^2)}$ ,

$$\xi_{k_M q}^{(h)}(x, y) = \frac{1}{\sqrt{(\epsilon_M - M_0)^2 + v^2 |k_M + i q|^2}} \begin{bmatrix} 0 \\ 0 \\ \epsilon_M - M_0 \\ -v(k_M + i q) \end{bmatrix} e^{i k_M x / \hbar} e^{i q y / \hbar}. \quad (4.4b)$$

The superconducting coupling mixes electron and hole components, which yields the solutions

$$\xi_{k_j q}^{(j1)}(x, y) = \frac{1}{\sqrt{\epsilon_j^2 + \Delta_0^2 + v^2 |k_j + i q|^2}} \begin{bmatrix} \Delta_0 e^{-i \phi_j} \\ 0 \\ -\epsilon_j \\ v(k_j + i q) \end{bmatrix} e^{i k_j x / \hbar} e^{i q y / \hbar}, \quad (4.5a)$$

$$\xi_{k_j q}^{(j2)}(x, y) = \frac{1}{\sqrt{\epsilon_j^2 + \Delta_0^2 + v^2 |k_j - i q|^2}} \begin{bmatrix} v(k_j - i q) \\ \epsilon_j \\ 0 \\ -\Delta_0 e^{i \phi_j} \end{bmatrix} e^{i k_j x / \hbar} e^{i q y / \hbar} \quad (4.5b)$$

for  $\epsilon_j = \sqrt{\Delta_0^2 + v^2 (k_j^2 + q^2)}$  in the left ( $j = L$ ) and right ( $j = R$ ) region.

Given fixed values of  $q$  and  $\epsilon$ , only transverse momenta  $k_M, k_j$  producing the correct energy are relevant, i. e. the solutions of the equations

$$k_M^2 = \frac{\epsilon^2 - M_0^2}{v^2} - q^2, \quad (4.6)$$

$$k_j^2 = \frac{\epsilon^2 - \Delta_0^2}{v^2} - q^2 = \begin{cases} k_M^2 - \frac{\Delta_0^2}{v^2}, & \text{if } M_0 = 0, \\ k_M^2, & \text{if } M_0 = \Delta_0. \end{cases} \quad (4.7)$$

The Hamiltonian is linear in the momentum  $\vec{p}$ , therefore the complete eigenmodes need to be continuous at the two boundaries  $x = \pm B/2$ . The natural length scale of the system,

$$\xi = \frac{\hbar v}{\Delta_0}, \quad (4.8)$$

will be relevant because we analyse the properties of the Josephson junction dependent on the width  $B$ .

## 4.3 SNS case

First, we will treat the SNS case,  $M \equiv 0$ .

### 4.3.1 Scattering states

Scattering states of fixed energy are conveniently characterised, e. g., by the longitudinal momentum  $q$  and the absolute value of the transversal momentum in the normal-conducting region,  $k_0 > \Delta_0/v$ :

$$\Rightarrow \epsilon = v \sqrt{k_0^2 + q^2} \quad (4.9)$$

In all three regions, waves can propagate in  $\pm x$  direction, therefore the relevant transversal momenta are  $\pm k_0$  in the middle region and

$$\pm k = \pm \sqrt{k_0^2 - \Delta_0^2/v^2} \quad (4.10)$$

in the superconducting areas. Hence, a piece-wise representation of the the wave function is given by

$$\Xi(x, y) = \sum_{\pm} \begin{cases} A_{(L1)}^{\pm} \xi_{\pm kq}^{(L1)}(x, y) + A_{(L2)}^{\pm} \xi_{\pm kq}^{(L2)}(x, y), & x < -B/2 \\ A_{(e)}^{\pm} \xi_{\pm k_0q}^{(e)}(x, y) + A_{(h)}^{\pm} \xi_{\pm k_0q}^{(h)}(x, y), & |x| < B/2 \\ A_{(R1)}^{\pm} \xi_{\pm kq}^{(R1)}(x, y) + A_{(R2)}^{\pm} \xi_{\pm kq}^{(R2)}(x, y), & B/2 < x \end{cases} \quad (4.11)$$

for a suitable choice of coefficients  $A$ . Given fixed values of  $k$  (or  $k_0$ ) and  $q$ , there are four independent solutions fulfilling the condition of continuity at the boundaries  $x = \pm B/2$ . They correspond, e. g., to the four incoming waves  $\xi_{+kq}^{(L1)}$ ,  $\xi_{+kq}^{(L2)}$ ,  $\xi_{-kq}^{(R1)}$  and  $\xi_{-kq}^{(R2)}$ . The boundary equations yield the transmission and reflection coefficients as well as the solutions in the ungapped middle.

To ensure a correct normalisation, we have to consider the system to be of finite size  $L_x L_y$  at first. For the case of a single ingoing wave, the corresponding coefficient needs to be chosen as

$$A_{\text{in}} = \frac{1}{\sqrt{L_x L_y}}. \quad (4.12)$$

In order to take the infinite-size limit, we have to replace sums over the momenta  $k, q$  with integrals. For integrands quadratic in the coefficients  $A$ , the lengths  $L_x$  and  $L_y$  cancel out in the end because they also appear in the integration measures.

### 4.3.2 Bound states

Now we consider the states localised in  $x$  direction. In the SNS junction, they consist of propagating waves in the normal-conducting middle area, but decay into both of the superconducting regions. The transversal momentum

$$\pm k_0 = \pm \frac{|m|}{v} \quad (4.13)$$

yields an effective mass term for the longitudinal wave in the energy:

$$\epsilon = \sqrt{m^2 + v^2 q^2}. \quad (4.14)$$

Although the transverse contribution to the energy has an upper bound  $m^2 < \Delta_0^2$ , the strict translation invariance in  $y$  direction means that the bound states in this model exist alongside the continuum of scattering states at energies  $\epsilon \geq \Delta_0$ , too. In the gapped regions, the momenta  $k_j$  are imaginary with the sign chosen to guarantee an exponential decay from the boundary,

$$i k_L = + \frac{\sqrt{\Delta_0^2 - m^2}}{v}, \quad (4.15)$$

$$i k_R = - \frac{\sqrt{\Delta_0^2 - m^2}}{v}, \quad (4.16)$$

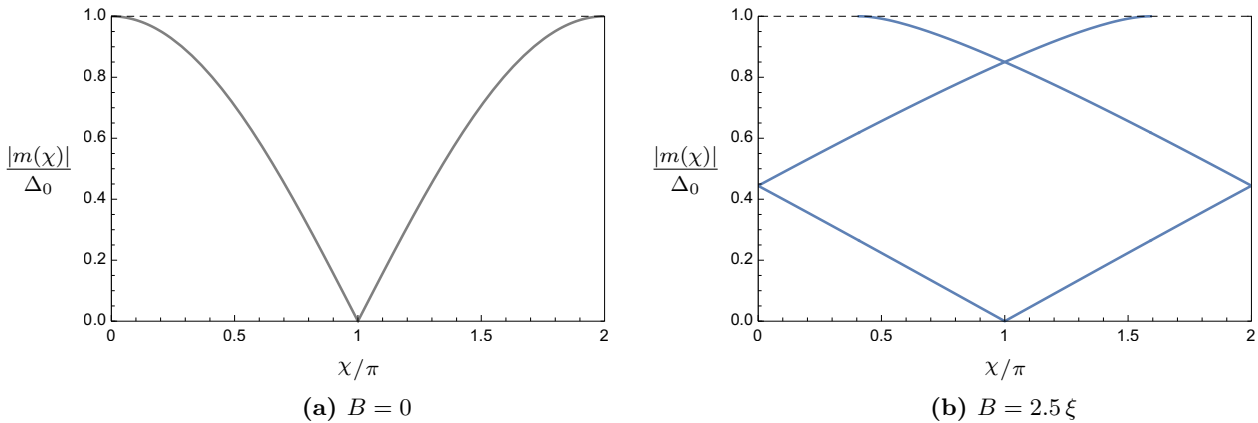


**Figure 4.2:** In the SNS case, the number of bound-state bands depends both on the junction width  $B$  and on the phase difference  $\chi$ . As a function of  $\chi$ , the mass  $m$  is given by a cosine in the limit of zero width (a). For wider junctions, bound-state bands merge with the continuum,  $|m(\chi)| \rightarrow \Delta_0$ , at certain combinations of  $B$  and  $\chi$  (b). The bound-state mass  $m$  is determined by the condition (4.18) and does not depend on the momentum  $q$  in the translation-invariant direction. As the sign of  $m$  has no impact, only the absolute value is shown here (see Fig. 4.3 for plots including sign).

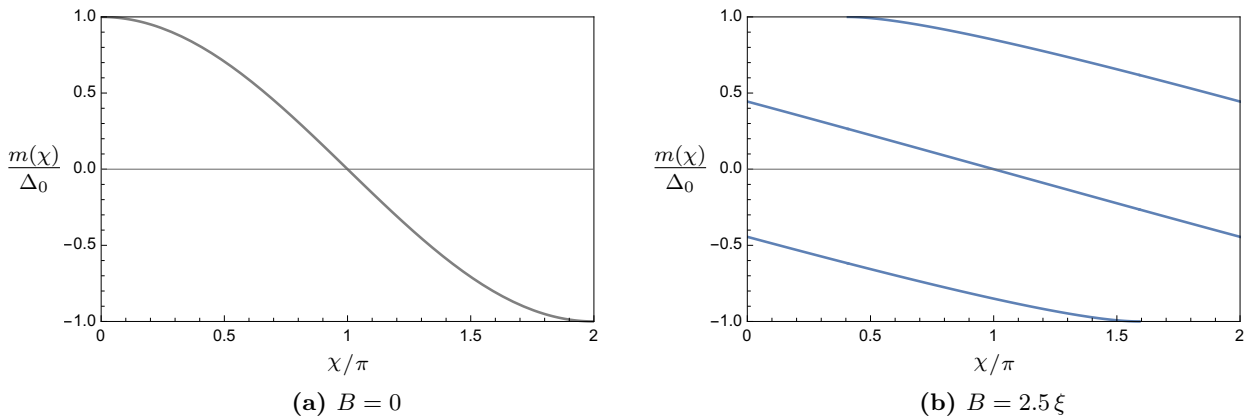


**Figure 4.3:** The sign of the bound-state mass  $m$  in the SNS case is arbitrary and has no physical relevance (see Fig. 4.2 for plots of the absolute value). As a signed quantity, however, the phase-dependence of  $m$  has the form of a single continuous curve for any junction width  $B$ . The function  $m(\chi)$  is given by a cosine in the zero-width limit (a). For finite junction width, the bound-state mass is not a single-valued function of phase; the number of solutions changes at certain combinations of  $B$  and  $\chi$  due to bound-state bands merging with the continuum:  $|m(\chi)| \rightarrow \Delta_0$  (b). The mass  $m$  is determined by the condition (4.18) has no dependence on the momentum  $q$ .

therefore the localised modes have the form

$$\Xi(x, y) = \begin{cases} A_{(L1)} \xi_{k_L q}^{(L1)}(x, y) + A_{(L2)} \xi_{k_L q}^{(L2)}(x, y), & x < -B/2 \\ \sum_{\pm} \left[ A_{(e)}^{\pm} \xi_{\pm k_0 q}^{(e)}(x, y) + A_{(h)}^{\pm} \xi_{\pm k_0 q}^{(h)}(x, y) \right], & |x| < B/2 \\ A_{(R1)} \xi_{k_R q}^{(R1)}(x, y) + A_{(R2)} \xi_{k_R q}^{(R2)}(x, y), & B/2 < x \end{cases} \quad (4.17)$$

The possible values for the mass  $m$  are restricted by the boundary conditions, as the wave function needs to be continuous at both boundary lines  $x = \pm B/2$  for a (non-trivial) set of coefficients  $A$ . This yields the quantisation condition

$$\exp \left[ i \frac{2 m B}{\hbar v} + i \chi \right] = \left( \frac{m + i \sqrt{\Delta_0^2 - m^2}}{\Delta_0} \right)^2, \quad (4.18)$$

which depends on the width of the junction  $B$  and the phase difference  $\chi$  between the superconducting regions. In general, there are multiple bands of bound states, which merge with the continuum at certain combinations of  $B$  and  $\chi$ . The sign of  $m$  is irrelevant for these calculations: both positive and negative  $m$  are allowed here. Figs. 4.2 and 4.3 illustrate the behaviour of the absolute values  $|m(\chi)|$  and the signed solutions  $m(\chi)$ , respectively.

As we can calculate the current contribution of the bound states from the  $\chi$  dependence of the energies (4.14) via the relation (4.18), we do not need normalised wave functions here. For completeness, let us remark that the infinite-size limit in  $y$  direction can be treated exactly like for the scattering states. Due to the condition (4.18), we retain a sum over discrete values of the transversal momentum, and the bound states are exponentially localised along  $x$  anyway.

### 4.3.3 Josephson current

The derivation of the Josephson current is explicated in App. D and App. E. For the scattering states, we calculate the contribution for momenta  $k, q$  by summing the expression (E.5) for the four incoming-wave solutions:

$$I_{\text{sc}}(k, q) = e v \sqrt{\frac{\Delta_0^2 + v^2 k^2}{\Delta_0^2 + v^2 (k^2 + q^2)}} L_y \sum_{j=1}^4 \left( |A_{(e)}^+|^2 - |A_{(e)}^-|^2 - |A_{(h)}^+|^2 + |A_{(h)}^-|^2 \right)_{j, kq}, \quad (4.19)$$

where an additional factor of the system size  $L_y$  comes from the translation-invariant  $y$  integral. Then, we integrate over both momenta in order to obtain the thermal expectation value of the current (E.14):

$$\mathcal{I}_{\zeta}^{\text{sc}} = -\frac{1}{2 \hbar^2} \int_0^{\infty} \frac{L_x}{2\pi} dk \int_0^{\zeta/v} \frac{2L_y}{2\pi} dq I_{\text{sc}}(k, q) \tanh \left( \frac{\sqrt{\Delta_0^2 + v^2 (k^2 + q^2)}}{2 k_B T} \right). \quad (4.20)$$

We have to introduce a cutoff at  $v q = \zeta \gg \Delta_0$  because the integral diverges; the additional factor of 2

replaces the integration over negative values of  $q$ . Using the expression

$$\frac{I_{\text{sc}}(k, q)}{L_y} = \frac{2ev}{L_x L_y} \sqrt{\frac{\Delta_0^2 + v^2 k^2}{\Delta_0^2 + v^2(k^2 + q^2)}} \frac{\Delta_0^2 v^2 k^2 \sin\left(2 \frac{B}{\hbar} \sqrt{k^2 + \frac{\Delta_0^2}{v^2}}\right) \sin(\chi)}{\left[ v^2 k^2 + \Delta_0^2 \sin^2\left(\frac{B}{\hbar} \sqrt{k^2 + \frac{\Delta_0^2}{v^2}} - \frac{\chi}{2}\right) \right] \left[ v^2 k^2 + \Delta_0^2 \sin^2\left(\frac{B}{\hbar} \sqrt{k^2 + \frac{\Delta_0^2}{v^2}} + \frac{\chi}{2}\right) \right]}, \quad (4.21)$$

the  $q$  integration can be carried out analytically for zero temperature:

$$\frac{\mathcal{I}_{\zeta}^{\text{sc}}}{L_y} \Big|_{T=0} = \frac{e}{\pi \hbar^2} \int_0^{\infty} \frac{dk}{2\pi} \sinh^{-1}\left(\frac{\zeta}{\sqrt{\Delta_0^2 + v^2 k^2}}\right) \frac{\Delta_0^2 v^2 k^2 \sqrt{\Delta_0^2 + v^2 k^2} \sin\left(2 \frac{B}{\hbar} \sqrt{k^2 + \frac{\Delta_0^2}{v^2}}\right) \sin(\chi)}{\left[ v^2 k^2 + \Delta_0^2 \sin^2\left(\frac{B}{\hbar} \sqrt{k^2 + \frac{\Delta_0^2}{v^2}} - \frac{\chi}{2}\right) \right] \left[ v^2 k^2 + \Delta_0^2 \sin^2\left(\frac{B}{\hbar} \sqrt{k^2 + \frac{\Delta_0^2}{v^2}} + \frac{\chi}{2}\right) \right]}. \quad (4.22)$$

For the bound states, we need to sum over solutions  $m_j$  of the quantisation condition (4.18). From this condition, we can determine the phase derivative

$$\frac{\partial m_j}{\partial \chi} = -\frac{1}{2} \frac{\sqrt{\Delta_0^2 - m_j^2}}{1 + \frac{B}{\hbar v} \sqrt{\Delta_0^2 - m_j^2}}, \quad (4.23)$$

which appears in the bound-state contributions (E.3) to the Josephson current (E.14):

$$\begin{aligned} \frac{\mathcal{I}_{\zeta}^{\text{b}}}{L_y} &= -\frac{e}{\hbar^2} \sum_{m_j} \int_0^{\zeta/v} \frac{dq}{\pi} \frac{\partial \epsilon}{\partial \chi} \tanh\left(\frac{\epsilon}{2 k_{\text{B}} T}\right) \\ &= -\frac{e}{\hbar^2} \sum_{m_j} \int_0^{\zeta/v} \frac{dq}{\pi} \frac{m_j}{\sqrt{m_j^2 + v^2 q^2}} \frac{\partial m_j}{\partial \chi} \tanh\left(\frac{\sqrt{m_j^2 + v^2 q^2}}{2 k_{\text{B}} T}\right), \end{aligned} \quad (4.24)$$

with the same  $q$  cutoff as for the scattering states. For zero-temperature, we obtain the expression

$$\frac{\mathcal{I}_{\zeta}^{\text{b}}}{L_y} \Big|_{T=0} \approx \frac{e}{2\pi \hbar^2 v} \sum_{m_j} \ln\left(\frac{2\zeta}{|m_j|}\right) \frac{m_j \sqrt{\Delta_0^2 - m_j^2}}{1 + \frac{B}{\hbar v} \sqrt{\Delta_0^2 - m_j^2}}. \quad (4.25)$$

Both the bound-state and the scattering-state contribution depend on the cutoff  $\zeta$ , but the divergent parts cancel each other. Therefore, the complete Josephson current per length is given by the limit of infinite cutoff:

$$\frac{\mathcal{I}_{\text{J}}(\chi)}{L_y} = \lim_{\zeta \rightarrow \infty} \frac{\mathcal{I}_{\zeta}^{\text{b}} + \mathcal{I}_{\zeta}^{\text{sc}}}{L_y}. \quad (4.26)$$

## 4.4 SMS case

When the magnetic gap is equal to the superconducting gap,  $M_0 = \Delta_0$ , the transversal momenta in the magnetic part are the same as in the superconduction regions.

### 4.4.1 Scattering states

The scattering states can be treated similar to the SNS case (Sec. 4.3.1). Due to  $k_M = k$ , we only have to replace  $k_0 \rightarrow k$  in the definition of the wave function (4.11), and we need to take into account that the energy is given by

$$\epsilon = \sqrt{\Delta_0^2 + v^2 (k^2 + q^2)} \quad (4.27)$$

for a state with longitudinal momentum  $q$  and absolute value of the transversal momentum  $k$ .

### 4.4.2 Bound states

Unlike in the SNS case, the transversal momentum  $k$  for the bound states is purely imaginary in all parts of the system. We use the effective mass  $m < \Delta_0$  in the energy

$$\epsilon = \sqrt{m^2 + v^2 q^2} \quad (4.28)$$

to express the absolute value of  $k$ :

$$ik = \sqrt{\Delta_0^2 - m^2} . \quad (4.29)$$

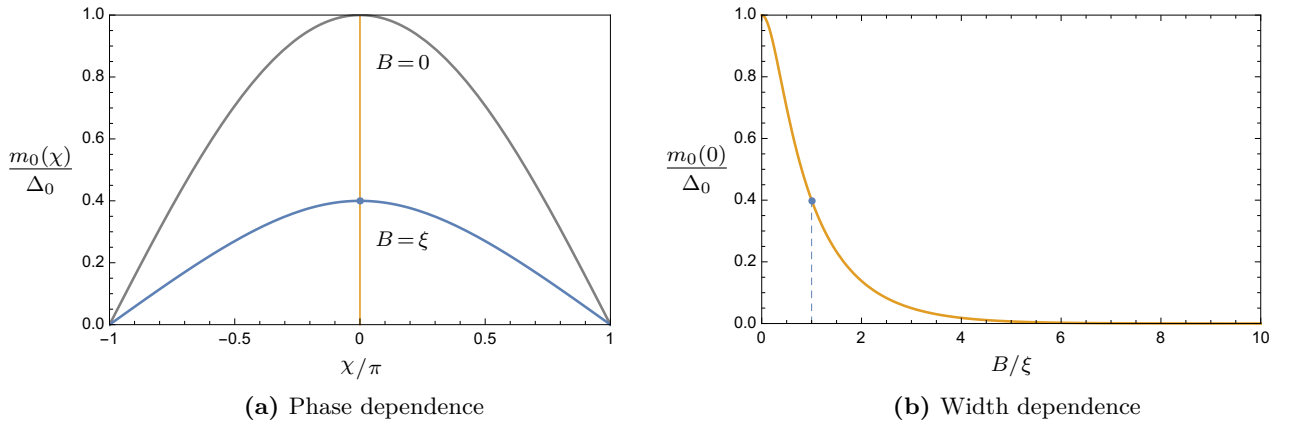


**Figure 4.4:** In the SMS case, there is always exactly one band of bound states. The phase-dependence of the mass  $m_0$  is unremarkable, although it deviates from the cosine shape for finite junction width (a). The maximum  $m_0(\chi = 0)$  is exponentially suppressed for larger junction widths  $B$  (b). The bound-state mass  $m$  is determined by the condition (4.31) and does not depend on the momentum  $q$  in the translation-invariant direction.

Bound-state wave functions are given by

$$\Xi(x, y) = \begin{cases} A_{(L1)} \xi_{+kq}^{(L1)}(x, y) + A_{(L2)} \xi_{+kq}^{(L2)}(x, y), & x < -B/2 \\ \sum_{\pm} \left[ A_{(e)}^{\pm} \xi_{\pm kq}^{(e)}(x, y) + A_{(h)}^{\pm} \xi_{\pm kq}^{(h)}(x, y) \right], & |x| < B/2 \\ A_{(R1)} \xi_{-kq}^{(R1)}(x, y) + A_{(R2)} \xi_{-kq}^{(R2)}(x, y), & B/2 < x \end{cases} . \quad (4.30)$$

Like in the SNS case of Sec. 4.3.2, there are bound states in the continuum for large values of the longitudinal momentum  $q$ , and the continuity constraint on the wave function yields a condition for the mass  $m$ :

$$m = \Delta_0 \cos\left[\frac{\chi}{2}\right] \exp\left[-\frac{B}{\hbar v} \sqrt{\Delta_0^2 - m^2}\right] . \quad (4.31)$$

The value of  $m(\Delta_0, B/v, \chi) \equiv m_0(\chi)$  is uniquely determined by this self-consistency equation (Fig. 4.4).

### 4.4.3 Josephson current

The Josephson current is calculated similar to the SNS case (cf. Sec. 4.3.3). Eq. (4.20) describes the integration over scattering-state contributions

$$I_{sc}(k, q) = \frac{e v^2 k}{\sqrt{\Delta_0^2 + v^2 (k^2 + q^2)}} L_y \sum_{j=1}^4 \left( |A_{(e)}^+|^2 - |A_{(e)}^-|^2 - |A_{(h)}^+|^2 + |A_{(h)}^-|^2 \right)_{j, kq}, \quad (4.32)$$

which are given by

$$\frac{I_{sc}(k, q)}{L_y} = \frac{2 e v}{L_x L_y} \frac{v k}{\sqrt{\Delta_0^2 + v^2 (k^2 + q^2)}} \cdot \frac{\Delta_0^2 (\Delta_0^2 + v^2 k^2) \sin[2 B k / \hbar] \sin[\chi]}{\left( v^2 k^2 + \Delta_0^2 \sin^2\left[\frac{\chi}{2}\right] \right)^2 + 4 \Delta_0^2 (\Delta_0^2 + v^2 k^2) \cos^2\left[\frac{\chi}{2}\right] \sin^2[B k / \hbar]} . \quad (4.33)$$

With a momentum cutoff at  $v q = \zeta \gg \Delta_0$ , this yields the zero-temperature current

$$\frac{\mathcal{I}_{\zeta}^{sc}}{L_y} \Big|_{T=0} = \frac{e}{\pi \hbar^2} \int_0^{\infty} \frac{dk}{2\pi} \sinh^{-1} \left( \frac{\zeta}{\sqrt{\Delta_0^2 + v^2 k^2}} \right) \cdot \frac{\Delta_0^2 (\Delta_0^2 + v^2 k^2) v k \sin[2 B k / \hbar] \sin[\chi]}{\left( v^2 k^2 + \Delta_0^2 \sin^2\left[\frac{\chi}{2}\right] \right)^2 + 4 \Delta_0^2 (\Delta_0^2 + v^2 k^2) \cos^2\left[\frac{\chi}{2}\right] \sin^2[B k / \hbar]} . \quad (4.34)$$

For the numerical evaluation in the following section, a symmetrical cutoff  $\Theta[\zeta^2 - v^2(k^2 + q^2)]$  turns out to be more expedient in this case. Using this alternative cutoff, we obtain

$$\frac{\mathcal{I}_\zeta^{\text{sc}}}{L_y} \Big|_{T=0} = \frac{e}{\pi \hbar^2} \int_0^{\zeta/v} \frac{dk}{2\pi} \ln \left( \frac{\sqrt{\Delta_0^2 + \zeta^2} + \sqrt{\zeta^2 - v^2 k^2}}{\sqrt{\Delta_0^2 + v^2 k^2}} \right) \cdot \frac{\Delta_0^2 (\Delta_0^2 + v^2 k^2) v k \sin[2Bk/\hbar] \sin[\chi]}{\left( v^2 k^2 + \Delta_0^2 \sin^2 \left[ \frac{\chi}{2} \right] \right)^2 + 4 \Delta_0^2 (\Delta_0^2 + v^2 k^2) \cos^2 \left[ \frac{\chi}{2} \right] \sin^2 [Bk/\hbar]} . \quad (4.35)$$

In the SMS system, there is only a single solution  $m_0$  of the quantisation condition (4.31) for the effective mass. When we insert the derivative

$$\frac{\partial m_0}{\partial \chi} = \frac{1}{2} \frac{m_0 \tan \left[ \frac{\chi}{2} \right]}{\frac{B}{\hbar v} \frac{m_0^2}{\sqrt{\Delta_0^2 - m_0^2}} - 1} \quad (4.36)$$

into the expression (4.24), we can write down the bound-state contribution for zero temperature:

$$\frac{\mathcal{I}_\zeta^{\text{b}}}{L_y} \Big|_{T=0} \approx \frac{e}{2\pi \hbar^2 v} \ln \left( \frac{2\zeta}{|m_0|} \right) \frac{m_0^2 \tan \left[ \frac{\chi}{2} \right]}{1 - \frac{B}{\hbar v} \frac{m_0^2}{\sqrt{\Delta_0^2 - m_0^2}}} . \quad (4.37)$$

The total current  $\mathcal{I}_J(\chi)$ , which is convergent in the SMS case, too, is defined by Eq. (4.26).

## 4.5 Zero-temperature results

At  $T = 0$ , the superconducting order parameter  $\Delta_0$  determines the energy scale of the problem. For the numerical evaluation, we construct dimensionless quantities by using both the length scale  $\xi$  and a dimensionful prefactor  $\mathcal{I}_0$  of the current:

$$\mathcal{I}_0 = \frac{e L_y \Delta_0^2}{\hbar^2 v} , \quad \xi = \frac{\hbar v}{\Delta_0} . \quad (4.38)$$

In the following, the current–phase relation is denoted by  $\mathcal{I}_J(\chi)$  with the derivative

$$\left. \frac{\partial \mathcal{I}_J}{\partial \chi} \right|_{\chi=0} \equiv \mathcal{I}'_J(0) . \quad (4.39)$$

The cutoff energy  $\zeta$  has to be chosen such that sufficient convergence of the limit (4.26) is achieved. Due to slower oscillations in the numerical integral, a larger value of  $\zeta$  is needed for smaller values of  $B/\xi$ . As the numerical integration is less stable for larger  $B$ , multiple cutoff values are used for the comparison of shapes in Fig. 4.5: It shows the current–phase relation  $\mathcal{I}_J(\chi)$ , normalised to a uniform slope at  $\chi = 0$ , for several values of  $B$ . In the SNS case, the deviation from the sinus shape increases with  $B/\xi$  (Fig. 4.5a), while the behaviour is non-monotonous in the magnetic case (Fig. 4.5b). As a numerical quantity characterising the change of shape, the ratio between the current at  $\chi = \frac{3\pi}{4}$  and the slope  $\mathcal{I}'_J(0)$  is depicted for both cases as a function of  $B$  in Fig. 4.6.

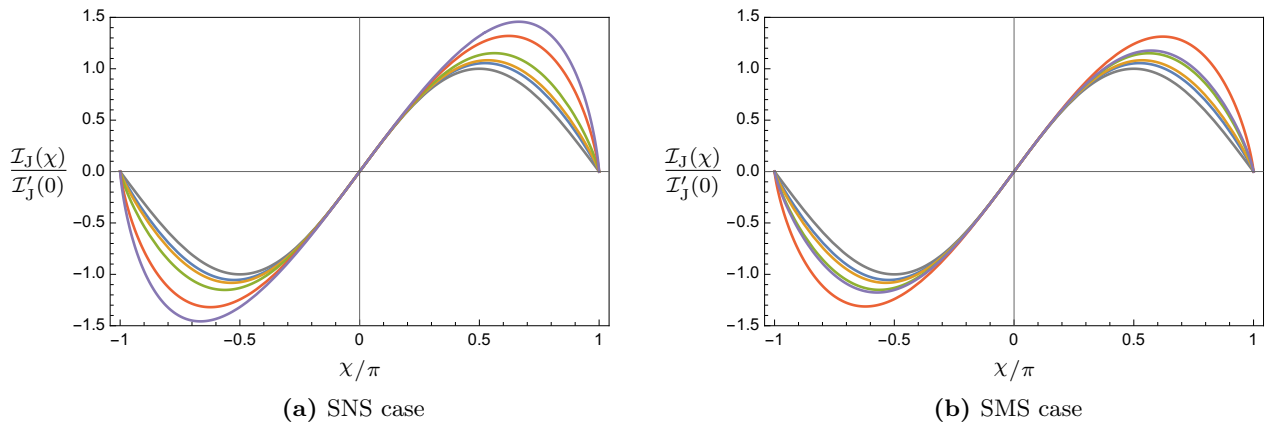


**Figure 4.5:** To illustrate the shape of the current–phase relation, curves are normalised to a uniform slope at  $\chi = 0$ . Additionally, a *sine* is plotted in *gray* for comparison. Values of  $B/\xi$ : 0.0003 (blue), 0.003 (orange), 0.03 (green), 0.3 (red), 3 (purple). Note that in the magnetic case (b), the shape changes non-monotonously (cf. Fig. 4.6).

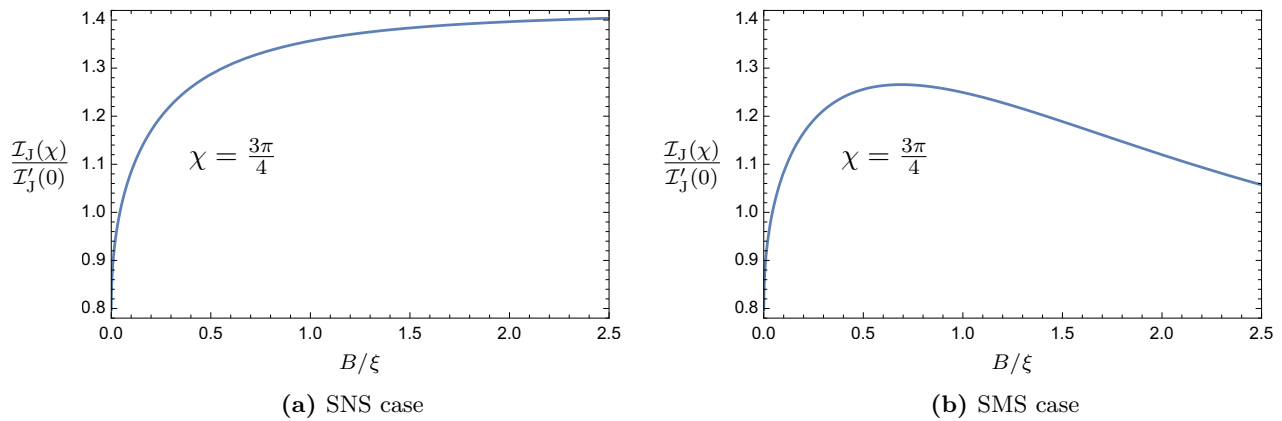


**Figure 4.6:** The ratio between the current at  $\chi = 3\pi/4$  and the slope at  $\chi = 0$  quantifies the change of shape (cf. Fig. 4.5). In the SMS case, the ratio is non-monotonous as a function of the junction width  $B$  (b). Plots for  $\zeta/\Delta_0 = 1000$ .

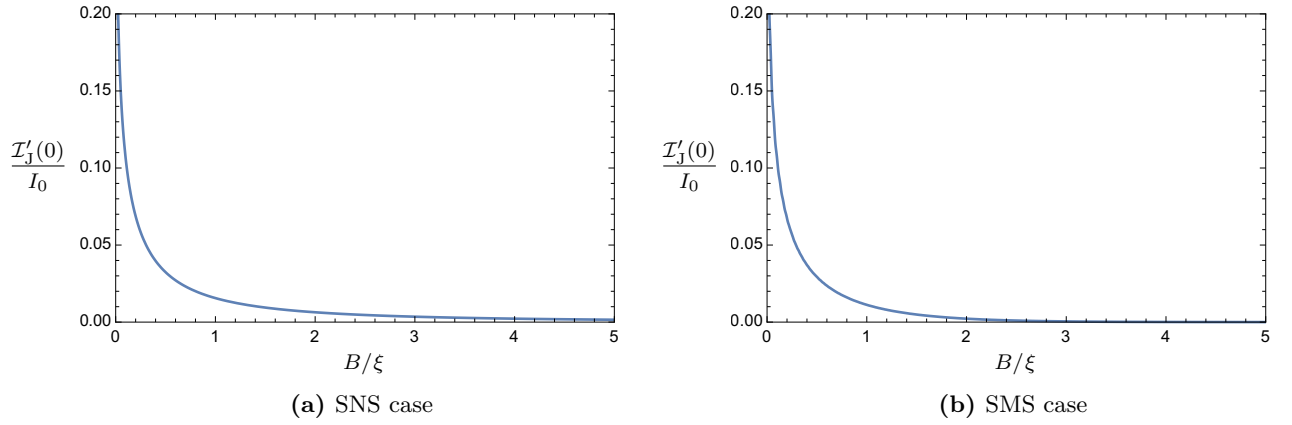


**Figure 4.7:** The slope at  $\chi = 0$  characterises the magnitude of the current, which decays faster (exponentially) as a function of the junction width  $B$  in the SMS case (see Fig. 4.8). Plots for  $\zeta/\Delta_0 = 100$ .

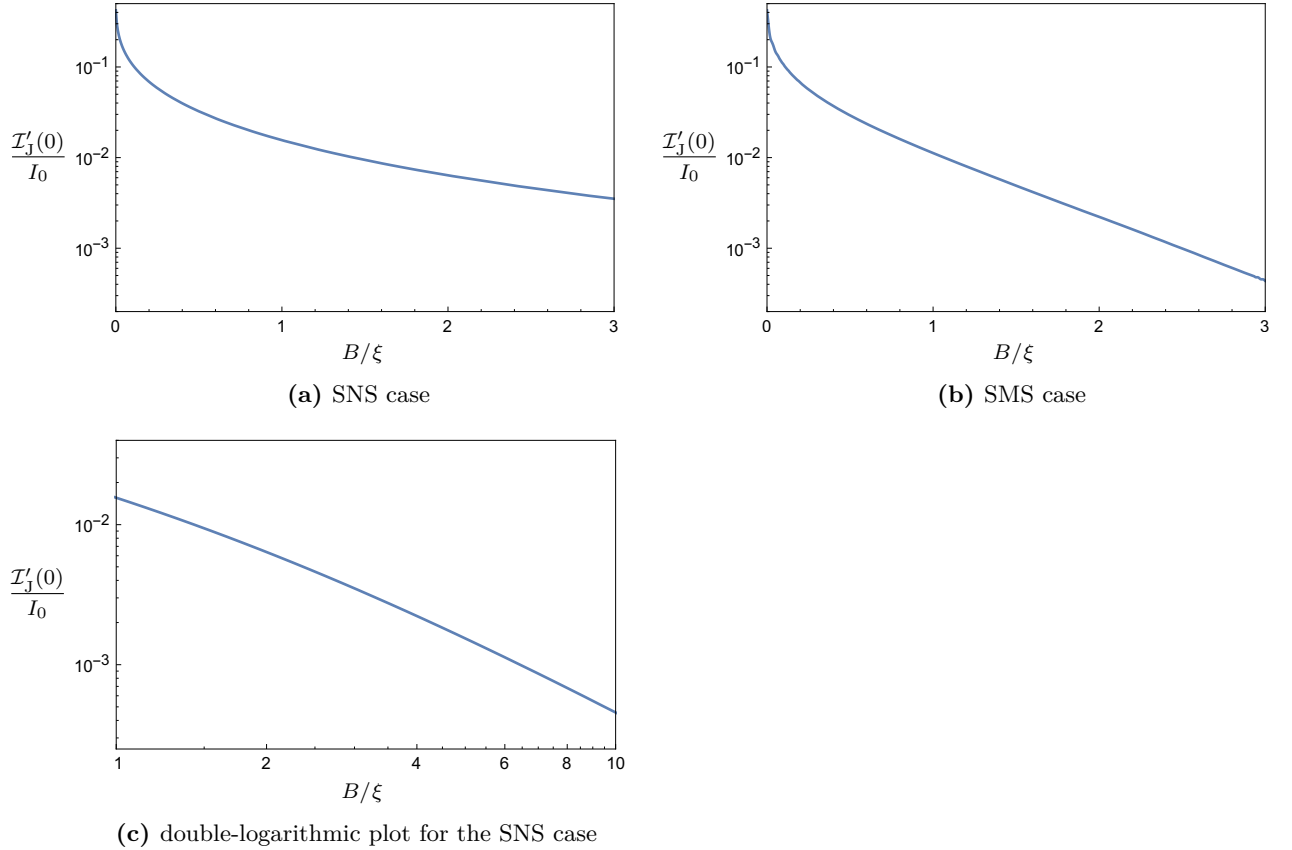


**Figure 4.8:** In the magnetic case, the dependence of the current on the junction width is given by an exponential decay (b). In contrast, the dependence looks approximately like a power law for larger values of  $B$  in the SNS case (c). Plots for  $\zeta/\Delta_0 = 100$ .

As a characteristic quantity for the magnitude of the current, the derivative  $\mathcal{I}'_J(0)$  is shown as a function of the junction width  $B$  in Fig. 4.7. The difference between non-magnetic and magnetic case is more visible in logarithmic plots: The magnitude of the current seems to have a power-law dependence in the SNS system, whereas it decays exponentially with  $B$  due to the magnetic gap in the SMS case (see Fig. 4.8). [In the SNS case, the contribution of bound states and the one of scattering modes individually show an oscillating behaviour, including sign changes. The simpler decay results only from the sum of both contributions.]

## 4.6 Conclusion

The limit  $\mu = 0$  of a long, translation-invariant Josephson junction on a TI surface has some peculiar properties. In particular, bound states are not restricted to energies below the continuum, which results in a logarithmically divergent contribution to the Josephson current. To compensate for that, the same divergence exists in the scattering-state contribution.  $4\pi$ -periodic current components do not appear in our calculation.

For larger junction widths  $B$ , the magnetic and non-magnetic cases differ significantly. In the SNS case, the current as a function of  $B$  behaves in a way similar to a non-topological superconductor–metal–superconductor junction, including oscillations in the contributions of bound states and of scattering modes which cancel each other [30, 31]. The magnetic case involves a simpler exponential decay of both contributions, but the shape of the current–phase relation changes in a non-monotonous and hence more complicated way.

In addition to the assumption  $\mu = 0$ , this calculation has another limitation: In general, the compensation of two logarithmic divergences is only possible if the linear spectrum of the topological insulator holds for an unlimited range of energy. The integration range that is effectively required to observe the compensation rises up to infinity when the junction width  $B$  is decreased to zero. Therefore, the behaviour of a more realistic system may deviate from this result for narrow junctions.



# 5 Chapter 5

---

## Summary and outlook

This thesis has discussed not only Majorana physics of fermions but also a spin analogue. There is a fundamental equivalence between a spin  $\frac{1}{2}$  and a fermionic mode, yet it is complicated by the difference in (anti-)commutation relations. Therefore, the well-known Jordan–Wigner transformation, which utilises non-local string operators to provide a spin–fermion mapping, is most useful for 1D problems. The extended transformation presented in Chap. 2 applies to *tree structures*, i. e. just slightly more than one-dimensional systems. In comparison to some more general proposals for spin–fermion transformations, however, it has the advantage that locality of Hamiltonians is strictly preserved and the complexity of couplings is increased only at vertices of the tree structure.

A larger tree structure is not necessary to perform *non-Abelian braiding* with Majorana zero modes, as a three-legged T geometry of topological wires is sufficient. For this special case of a star graph, an extended Jordan–Wigner transformation was already introduced in Ref. [18]. Although the spin chains lack the topological protection of a delocalised fermionic zero mode, Majorana braiding operations can be translated from the fermionic language into a *spin representation* for this system (cf. App. A). This representation might be useful for simulating fermions and fermionic quantum computation with ordinary, bosonic qubits.

Spatially separate Majorana zero modes can be considered to form non-local fermionic states, but this alone does not result in correlations between the different regions of a system. This is evident from the fact that, in a universe with multiple pairs of zero-energy Majorana modes, the choice of pairs for defining the non-local fermions is arbitrary, in principle. A physically relevant connection in the Hamiltonian is created, for instance, by the *Coulomb interaction* on a topologically superconducting island of mesoscopic size. The correlation due to this interaction between Majorana-mediated currents at two tunnel contacts can be analysed for a small charging energy in the formalism of an effective phase action, as done in Chap. 3.

The chapters above discussed only (nearly) one-dimensional systems and exponentially localised, virtually zero-dimensional Majorana bound states. A different setting is the subject of Chap. 4: A three-dimensional *topological insulator* has a gapped bulk, but protected gapless states on the surface, so it provides an effectively 2D system of electrons. An additional feature of the surface states is their relativistic Dirac spectrum. Proximity to a magnetic material can induce a gap at the Dirac point, while a proximity-induced superconducting order parameter gaps the spectrum at the chemical potential.

In a *Josephson junction* between two superconductors on the topological-insulator surface, this effect on the spectrum implies that the surface states have an influence on the Josephson current. If the

superconductors are separated by a vacuum or a magnetic insulator likewise deposited on the surface, direct tunneling between the superconductors is suppressed exponentially in their distance. This means that contributions of surface states, including one-dimensional *Majorana edge modes* localised around the junction, are important for the Josephson current.

In addition to a gap opening in a magnetic region, the *translation-invariant* direction along the junction decouples completely from the perpendicular direction for a chemical potential at the Dirac point, which has been considered in Chap. 4. Hence, assuming an unlimited range of the Dirac spectrum, there are bound states at arbitrarily large energies with logarithmic divergencies that cancel each other in bound-state and scattering-state contributions to the Josephson current. This makes the combination of a translation-invariant junction geometry with a chemical potential at the Dirac point of a relativistic spectrum a rather unusual case.

In conclusion, topological superconducting systems feature a variety of different Majorana modes. Chiral and non-chiral realisations of one-dimensional Majorana states, which may be easier to probe and control in experiment than the zero modes in superconducting vortices, are particularly interesting examples. While there have been proposals for interferometric studies of topological Majorana modes for more than a decade (e. g. Ref. [10]), research activity has been encouraged by experimental progress, with some recent findings indicating a detection of Majorana edge modes [32, 33]. An implementation of non-Abelian braiding with propagating 1D states of Majorana character would be a very intriguing prospect. Both about physical realisation and manipulation and in theoretical description, at any rate, there are still many open questions that remain to be explored.

# A Majorana braiding in spin representation

The modified Jordan–Wigner transformation of Chap. 2 allows for the translation of Majorana braiding into the language of spin systems. The spin system corresponding to a fermionic T junction of Kitaev chains (Sec. 1.3) is introduced in the first part of this appendix. Boundary translations allowed me to describe a Majorana phase-gate operation in a purely one-dimensional geometry in my master’s thesis (cf. Ref. [13]). As defined in the second part of this appendix, they are used, in the third part, to explicate the spin representation of a braiding operation for a single topological interval. The final part provides a detailed calculation for the spin equivalent of braiding Majorana modes from two separate topological intervals. Results contained in this appendix have been published in Refs. [13] and [14].

## A.1 Geometry

The generalised Jordan–Wigner transformation defined in Eqs. (2.13) and Sec. 2.3 yields a spin representation for a fermionic T junction of Kitaev chains (cf. Sec. 1.3):

$$H = \sum_{\alpha=1}^3 H_{0,\alpha} + H_{\text{int}}^S \quad (\text{A.1a})$$

$$H_{0,\alpha} = - \sum_{j=1}^{L_\alpha} h_\alpha(j) \sigma_\alpha^x(j) - J \sum_{j=1}^{L_\alpha-1} \sigma_\alpha^z(j) \sigma_\alpha^z(j+1) \quad (\text{A.1b})$$

$$H_{\text{int}}^S = -\frac{1}{2} \sum_{\alpha\beta\gamma} |\epsilon^{\alpha\beta\gamma}| J_{\alpha\beta} S_0^\gamma \sigma_\alpha^z(1) \sigma_\beta^z(1), \quad (\text{A.1c})$$

a system of Ising spin chains with a local transverse magnetic field  $h_\alpha(j)$ , which corresponds to a locally tunable chemical potential in the fermionic system. Assuming  $J > 0$ , any interval of spins with  $|h| \ll J$  in one of the chains is ferromagnetic, whereas  $|h| \gg J$  results in a trivial (paramagnetic) phase. The three chains are linked by the components of an additional central spin  $S_0$  via 3-spin couplings of strength  $J_{\alpha\beta} = J_{\beta\alpha}$ . This structure is depicted in Fig. A.1.

The in-depth examination of the braiding in the following sections will be restricted to an *ideal case*:  $h = 0$  in the topological regions (spins aligned along the  $z$  axis) and  $h = \infty$  in the rest of the chain (all spins point in  $+x$  direction). Thereby outside the topological regions, pairs  $\gamma_\alpha(2j-1)$  and  $\gamma_\alpha(2j)$  belonging to spin  $\sigma_\alpha(j)$  constitute a fermionic mode, while Majorana operators  $\gamma_\alpha(2j)$  and  $\gamma_\alpha(2j+1)$  of consecutive spins are paired in the topological intervals. This leaves two operators at the boundaries

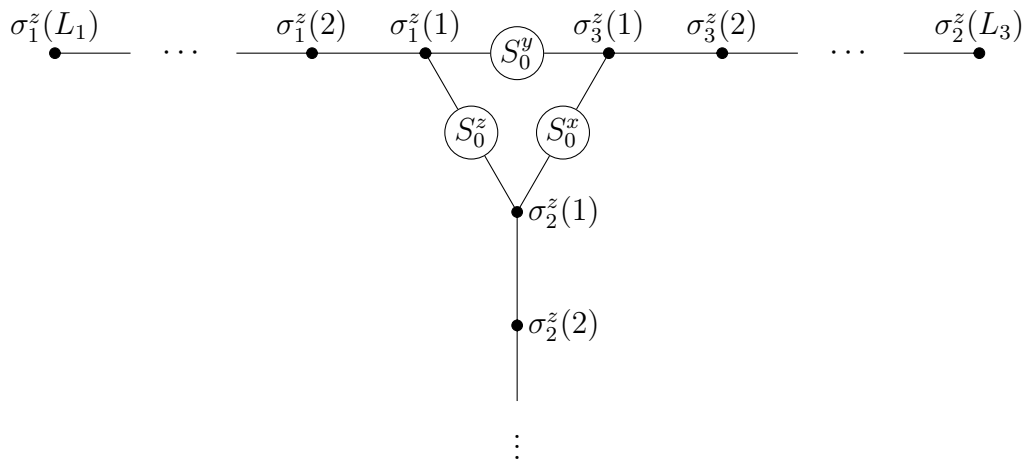


**Figure A.1:** Ising spin chains in a T geometry. A fermionic T junction suitable for Majorana braiding (Sec. 1.4) has a spin representation of this structure, which is described by the Hamiltonian in Eqs. (A.1). The couplings between three Ising spin chains are mediated by the components of an additional spin  $S_0$ , cf. Ref. [18] and Sec. 2.3. The system can be manipulated by tuning transverse fields (not depicted here) that act on the individual spins  $\sigma_\alpha(j)$  of the three chains.

of each interval to form a zero-energy mode (cf. Sec. 1.3), therefore the groundstate degeneracy is 2 to the power of the number of intervals.

In a fermionic T geometry, a braiding operation is effected by moving two Majorana zero modes in such a way that they swap positions (cf. Sec. 1.4). The boundaries of topological intervals can be shifted by local tuning of the chemical potential, which corresponds to the magnetic field in the spin system. Assuming  $J_{12} = J_{13} = J_{23} > 0$  for symmetry, we will consider the spin equivalent for both the braiding of the two Majorana zero modes from a single topological interval and a braiding operation between two different intervals.

## A.2 Boundary translations

For the ideal case we analyse here, it is easy to describe, e. g., a shift of the inner boundary of an interval towards the coupler, from spin  $\sigma_\alpha(k+1)$  to  $\sigma_\alpha(k)$ , due to a suitable adiabatic change of field  $h_k$ :

$$T_\alpha^{\text{in}}(k) = \exp\left[i\frac{\pi}{4}\sigma_\alpha^y(k)\sigma_\alpha^z(k+1)\right] = \frac{1 + i\sigma_\alpha^y(k)\sigma_\alpha^z(k+1)}{\sqrt{2}}. \quad (\text{A.2})$$

This unitary operator merely rotates  $\sigma_\alpha(k)$  from the  $x$  direction to  $\pm z$  direction dependent on the orientation of  $\sigma_\alpha(k+1)$ . Similarly, we construct the operator describing a shift of an outer interval boundary away from the coupler, from spin  $\sigma_\alpha(k)$  to  $\sigma_\alpha(k+1)$ :

$$T_\alpha^{\text{out}}(k) = \exp\left[i\frac{\pi}{4}\sigma_\alpha^y(k+1)\sigma_\alpha^z(k)\right] = \frac{1 + i\sigma_\alpha^y(k+1)\sigma_\alpha^z(k)}{\sqrt{2}}. \quad (\text{A.3})$$

If the shift goes across the coupler  $S_0$ , transforming an inner boundary on chain  $\alpha$  into an outer boundary on chain  $\beta$ , the coupler state determines the ferromagnetic or anti-ferromagnetic alignment

of the spins. Therefore this translation is given by

$$T_{\beta\leftarrow\alpha} = \exp\left[i\frac{\pi}{4}|\epsilon^{\alpha\beta\gamma}|S_0^\gamma\sigma_\beta^y(1)\sigma_\alpha^z(1)\right] = \frac{1+i|\epsilon^{\alpha\beta\gamma}|S_0^\gamma\sigma_\beta^y(1)\sigma_\alpha^z(1)}{\sqrt{2}}. \quad (\text{A.4})$$

with an implied summation over the index  $\gamma$ . In the fermionic representation, the coupler does not appear. It is important to note, however, that the Jordan–Wigner transformation (2.13) results in non-trivial commutation relations between coupler components and fermion operators.

As long as the two boundaries of an interval do not meet, translations of the inner boundary commute with translations of the outer one, because the former (the latter) involve only odd-numbered (even-numbered) Majorana operators. Obviously, boundary translations on different chains commute, too. Therefore we can describe a translation of a topological interval, e. g. from chain  $\alpha$  to chain  $\beta$ , by a shift of the inner boundary on chain  $\alpha$  to its final position as outer boundary on chain  $\beta$ , followed by a shift of the other boundary, regardless of the actual specific procedure.

### A.3 Single-interval braiding

Without loss of generality, we assume that the ferromagnetic interval is positioned on the first chain at the start of the procedure. In order to effect a braiding operation, the whole interval needs to be shifted, e. g., first to the second chain, then to the third chain and finally back to the first chain.

On each of the chains  $\alpha$ , the interval boundaries will be moved to the position between spin indices  $N_\alpha^{\text{in}}$  and  $N_\alpha^{\text{out}}$ . We construct the complete braiding operation from the three interval movements:

$$U_{\text{br}} = U_{13} U_{32} U_{21}. \quad (\text{A.5})$$

Each of the movements consists of translations of the two boundaries:

$$U_{\beta\alpha} = \left[T_{\alpha,\text{out}} T_{\alpha\leftarrow\beta} T_{\beta,\text{in}}\right]^\dagger \cdot T_{\beta,\text{out}} T_{\beta\leftarrow\alpha} T_{\alpha,\text{in}}, \quad (\text{A.6})$$

where elementary boundary translations from Sec. A.2 are used to construct the operators

$$T_{\alpha,\text{in}} = \prod_{j=1}^{j=N_\alpha^{\text{in}}} T_\alpha^{\text{in}}(j) \quad (\text{A.7})$$

and

$$T_{\alpha,\text{out}} = \prod_{j=N_\alpha^{\text{out}}}^{j=1} T_\alpha^{\text{out}}(j). \quad (\text{A.8})$$

As operators  $T$  are unitary and  $T_{\alpha,\text{out}}$  contain only the  $z$  component  $\sigma_\alpha^z(1)$  for the first spin of the chain, many terms cancel immediately:

$$\Rightarrow U_{\text{br}} = T_{1,\text{in}}^\dagger T_{1,\text{out}} \cdot T_{3\leftarrow 1}^\dagger T_{1\leftarrow 3} T_{2\leftarrow 3}^\dagger T_{3\leftarrow 2} T_{1\leftarrow 2}^\dagger T_{2\leftarrow 1} \cdot T_{1,\text{out}}^\dagger T_{1,\text{in}}. \quad (\text{A.9})$$

For further analysis, we make use of our preexisting knowledge about the operation. All spins in the second and third chain, in particular  $\sigma_2(1)$  and  $\sigma_3(1)$ , are frozen into  $+x$  direction at the start and end of the operation. Using projectors for the  $+x$  alignment of these spins,

$$P_\alpha^{+x}(j) = \left|\sigma_\alpha^{+x}(j)\right\rangle \left\langle\sigma_\alpha^{+x}(j)\right|, \quad (\text{A.10})$$

we need to take into account only terms preserving this alignment of  $\sigma_2(1)$  and  $\sigma_3(1)$ :

$$\begin{aligned}
& P_2^{+x}(1) P_3^{+x}(1) \cdot \left[ T_{3\leftarrow 1}^\dagger T_{1\leftarrow 3} T_{2\leftarrow 3}^\dagger T_{3\leftarrow 2} T_{1\leftarrow 2}^\dagger T_{2\leftarrow 1} \right] \cdot P_3^{+x}(1) P_2^{+x}(1) \\
&= \frac{1}{4} P_2^{+x}(1) P_3^{+x}(1) \left[ 1 + \sigma_1^x(1) \sigma_2^x(1) + \sigma_1^x(1) \sigma_3^x(1) + \sigma_2^x(1) \sigma_3^x(1) \right] P_3^{+x}(1) P_2^{+x}(1) \\
&\quad + \frac{i}{4} P_2^{+x}(1) P_3^{+x}(1) \left[ \sigma_1^x(1) \sigma_2^x(1) \sigma_3^x(1) + \sigma_1^x(1) - \sigma_2^x(1) - \sigma_3^x(1) \right] P_3^{+x}(1) P_2^{+x}(1) \\
&= \frac{1 + \sigma_1^x(1)}{2} P_3^{+x}(1) P_2^{+x}(1) - i \frac{1 - \sigma_1^x(1)}{2} P_3^{+x}(1) P_2^{+x}(1) \\
&= e^{-i\frac{\pi}{4}} \frac{1 + i\sigma_1^x(1)}{\sqrt{2}} P_3^{+x}(1) P_2^{+x}(1) . \tag{A.11}
\end{aligned}$$

As the projectors have removed any dependence on the spins of the second and third chain, they are not important for the remaining calculation.

Neither  $T_{1,\text{in}}$  nor  $T_{1,\text{out}}$  commute with the operator  $\sigma_1^x(1)$ . Therefore, we have to look at the boundary translations of the first chain in detail. The anti-commutation relations between spin operators can invert boundary translations,

$$\sigma_\alpha^x(k) \left[ T_\alpha^{\text{out}}(k) \right]^\dagger = T_\alpha^{\text{out}}(k) \sigma_\alpha^x(k) , \tag{A.12}$$

and the squares of the translations are given by

$$\left[ T_\alpha^{\text{in}}(k) \right]^2 = i \sigma_\alpha^y(k) \sigma_\alpha^z(k+1) , \tag{A.13}$$

$$\left[ T_\alpha^{\text{out}}(k) \right]^2 = i \sigma_\alpha^y(k+1) \sigma_\alpha^z(k) . \tag{A.14}$$

The  $\sigma_1^x(1)$  term can be calculated by commuting the boundary translations individually. In the following, the terms we commute to a different position are highlighted in **blue** at their old location and in **red** at their new one. The factor that has been relevant for the anti-commutation behaviour is printed in **bold**:

$$\begin{aligned}
& T_{1,\text{in}}^\dagger T_{1,\text{out}} \cdot \sigma_1^x(1) \cdot T_{1,\text{out}}^\dagger T_{1,\text{in}} \\
&= T_{1,\text{in}}^\dagger \cdot T_1^{\text{out}}(N_1^{\text{out}}) \dots T_1^{\text{out}}(2) \cdot T_1^{\text{out}}(1) \cdot \sigma_1^x(1) \cdot \left[ T_1^{\text{out}}(1) \right]^\dagger \left[ T_1^{\text{out}}(2) \right]^\dagger \dots \left[ T_1^{\text{out}}(N_1^{\text{out}}) \right]^\dagger \cdot T_{1,\text{in}} \\
&= T_{1,\text{in}}^\dagger \cdot T_1^{\text{out}}(N_1^{\text{out}}) \dots T_1^{\text{out}}(2) \left[ T_1^{\text{out}}(1) \right]^2 \cdot \sigma_1^x(1) \cdot \left[ T_1^{\text{out}}(2) \right]^\dagger \left[ T_1^{\text{out}}(3) \right]^\dagger \dots \left[ T_1^{\text{out}}(N_1^{\text{out}}) \right]^\dagger \cdot T_{1,\text{in}} \\
&= T_{1,\text{in}}^\dagger \cdot T_1^{\text{out}}(N_1^{\text{out}}) \dots T_1^{\text{out}}(3) \left[ T_1^{\text{out}}(2) \right]^2 \left[ T_1^{\text{out}}(1) \right]^2 \cdot \sigma_1^x(1) \cdot \left[ T_1^{\text{out}}(3) \right]^\dagger \dots \left[ T_1^{\text{out}}(N_1^{\text{out}}) \right]^\dagger \cdot T_{1,\text{in}} .
\end{aligned}$$

By continuing in this fashion, we obtain

$$\begin{aligned}
T_{1,\text{in}}^\dagger T_{1,\text{out}} \cdot \sigma_1^x(1) \cdot T_{1,\text{out}}^\dagger T_{1,\text{in}} &= T_{1,\text{in}}^\dagger \cdot \prod_{j=N_1^{\text{out}}}^{j=1} \left[ T_1^{\text{out}}(j) \right]^2 \cdot \sigma_1^x(1) \cdot T_{1,\text{in}} \\
&= \prod_{j=N_1^{\text{out}}}^{j=1} \left[ T_1^{\text{out}}(j) \right]^2 \cdot T_{1,\text{in}}^\dagger \cdot \sigma_1^x(1) \cdot T_{1,\text{in}} , \tag{A.15}
\end{aligned}$$

which allows us to treat the translations of the inner boundary in a similar way:

$$\begin{aligned}
& T_{1,\text{in}}^\dagger \cdot \sigma_1^x(1) \cdot T_{1,\text{in}} \\
&= [T_1^{\text{in}}(N_1^{\text{in}})]^\dagger \cdots [T_1^{\text{in}}(2)]^\dagger [T_1^{\text{in}}(1)]^\dagger \cdot \sigma_1^x(1) \cdot T_1^{\text{in}}(1) T_1^{\text{in}}(2) \cdots T_1^{\text{in}}(N_1^{\text{in}}) \\
&= [T_1^{\text{in}}(N_1^{\text{in}})]^\dagger \cdots [T_1^{\text{in}}(3)]^\dagger [T_1^{\text{in}}(2)]^\dagger \cdot \sigma_1^x(1) \cdot [T_1^{\text{in}}(1)]^2 T_1^{\text{in}}(2) \cdots T_1^{\text{in}}(N_1^{\text{in}}) \\
&= [T_1^{\text{in}}(N_1^{\text{in}})]^\dagger \cdots [T_1^{\text{in}}(3)]^\dagger \cdot \sigma_1^x(1) \cdot [\mathbf{T}_1^{\text{in}}(1)]^2 [T_1^{\text{in}}(2)]^2 T_1^{\text{in}}(3) \cdots T_1^{\text{in}}(N_1^{\text{in}}) \\
&= \dots = \sigma_1^x(1) \cdot \prod_{j=1}^{j=N_1^{\text{in}}} [T_1^{\text{in}}(j)]^2 .
\end{aligned} \tag{A.16}$$

For the complete  $\sigma_1^x(1)$  term, this yields

$$\begin{aligned}
& T_{1,\text{in}}^\dagger T_{1,\text{out}} \cdot \sigma_1^x(1) \cdot T_{1,\text{out}}^\dagger T_{1,\text{in}} \\
&= \prod_{j=N_1^{\text{out}}}^{j=1} [T_1^{\text{out}}(j)]^2 \cdot \sigma_1^x(1) \cdot \prod_{j=1}^{j=N_1^{\text{in}}} [T_1^{\text{in}}(j)]^2 \\
&= i \sigma_1^y(N_1^{\text{out}} + 1) \cdot \prod_{j=N_1^{\text{out}}}^{j=2} \sigma_1^x(j) \cdot \sigma_1^z(1) \cdot \sigma_1^x(1) \cdot \sigma_1^y(1) \cdot \prod_{j=2}^{j=N_1^{\text{in}}} \sigma_1^x(j) \cdot i \sigma_1^z(N_1^{\text{in}} + 1) \\
&= \sigma_1^z(N_1^{\text{in}} + 1) \sigma_1^z(N_1^{\text{out}} + 1) \prod_{j=N_1^{\text{in}}+1}^{j=N_1^{\text{out}}+1} \sigma_1^x(j) .
\end{aligned} \tag{A.17}$$

Remembering the expression (A.11), we can now write down the effective braiding operator:

$$U_{\text{br}} = \frac{e^{-i \frac{\pi}{4}}}{\sqrt{2}} \left[ 1 + i \sigma_1^z(N_1^{\text{in}} + 1) \sigma_1^z(N_1^{\text{out}} + 1) \prod_{j=N_1^{\text{in}}+1}^{j=N_1^{\text{out}}+1} \sigma_1^x(j) \right] \tag{A.18}$$

This result is compatible with the expression (2.15) for  $\gamma_A = \gamma(2 N_1^{\text{in}} + 1)$  and  $\gamma_B = \gamma(2 N_1^{\text{out}} + 2)$ . Even though the state of the coupler is unchanged after the braiding operation, the coupler spin undergoes non-trivial dynamics (and entanglement with the ferromagnetic interval) during braiding, which results in the additional phase factor in Eq. (A.18).

The fermionic parity of the topological interval is conserved in the braiding operation. Therefore, the eigenstates  $|\pm\rangle$  of the fermionic parity operator for the topological zero mode,

$$i \gamma_A \gamma_B = \sigma_1^z(N_1^{\text{in}} + 1) \sigma_1^z(N_1^{\text{out}} + 1) \prod_{j=N_1^{\text{in}}+1}^{j=N_1^{\text{out}}+1} \sigma_1^x(j) , \tag{A.19}$$

with  $i \gamma_A \gamma_B |\pm\rangle = \pm |\pm\rangle$ , are the eigenstates of the braiding operation  $U_{\text{br}}$ :

$$|+\rangle \equiv |0\rangle = \frac{|\uparrow\uparrow\uparrow\rangle + |\downarrow\downarrow\downarrow\rangle}{\sqrt{2}} , \tag{A.20a}$$

$$|-\rangle \equiv |1\rangle = \frac{|\uparrow\uparrow\uparrow\rangle - |\downarrow\downarrow\downarrow\rangle}{\sqrt{2}} . \tag{A.20b}$$

Here, only the spin alignment of the ferromagnetic interval is indicated.

During the whole operation, at most one of the three-spin couplings in  $H_{\text{int}}^S$  from Eq. (A.1c) is needed. Therefore it is possible to emulate the braiding process in the purely one-dimensional geometry of only two spin chains by including controlled rotations of the coupler spin into the protocol (see Ref. [13]).

## A.4 Two-interval braiding

Now we consider the spin equivalent of braiding Majorana modes of two topological intervals in the fermionic system. For each interval, only one of the boundaries is shifted in this process, so the spins contained in the intervals from the start do not change their alignment, unlike in the single-interval process. However, two-interval braiding cannot be effected in such a way that at most one of the 3-spin couplings in Eq. (A.1c) is relevant at each step. Therefore, the *coupler spin*  $S_0$  is necessarily rotated in the process, which we will examine in the following.

The topological intervals and adiabatic shifts of their boundaries within a fermionic chain can be translated to the ferromagnetic intervals in the spin representation exactly like for the case of a single topological interval (Sec. A.3). At the beginning, the ferromagnetic intervals have to be prepared, e. g., in the first and third chain in some distance to the coupler spin  $S_0$ . At first, we consider an initial state with the spins in both intervals as well as the coupler aligned in  $+z$  direction:

$$|\psi_0\rangle = |\uparrow\uparrow\uparrow\odot\rangle_1 \otimes |\odot\odot\rangle_2 \otimes |\odot\uparrow\uparrow\uparrow\rangle_3 \otimes |S_0\uparrow\rangle. \quad (\text{A.21})$$

Here the indices denote the three spin chains; the corresponding arrows indicate the spin orientation in ferromagnetic ( $\uparrow/\downarrow$ ) and paramagnetic areas ( $\odot$ ). Their alignment roughly symbolises the locations of the intervals in the T-junction geometry, but this calculation does not depend on the specific interval lengths and distances to the coupler (thought to be in the middle above the second chain as shown in Fig. A.1). The first step comprises shifting the right boundary of the first interval (i. e. one Majorana mode in the fermionic system) onto the second chain, resulting in the state

$$|\psi_1\rangle = |\odot\uparrow\uparrow\uparrow\rangle_1 \otimes |\uparrow\uparrow\rangle_2 \otimes |\odot\uparrow\uparrow\uparrow\rangle_3 \otimes |S_0\uparrow\rangle. \quad (\text{A.22})$$

If the coupler state were  $|S_0\downarrow\rangle$ , the spins in the second chain would just be flipped compared to those in the first chain.

The non-trivial part begins when the second interval is also shifted to the junction. While the spin alignments of the ferromagnetic intervals stay fixed, the coupler spin rotates to adjust to the change of its effective magnetic field from the  $z$  direction  $\begin{pmatrix} 0 \\ 0 \\ 1 \end{pmatrix}$  about the axis  $\vec{a} = \frac{1}{\sqrt{2}} \begin{pmatrix} 1 \\ -1 \\ 0 \end{pmatrix}$  to the space diagonal  $\frac{1}{\sqrt{3}} \begin{pmatrix} 1 \\ 1 \\ 1 \end{pmatrix}$ :

$$\begin{aligned} \Rightarrow |\psi_2\rangle &= |\odot\uparrow\uparrow\uparrow\rangle_1 \otimes |\uparrow\uparrow\rangle_2 \otimes |\uparrow\uparrow\uparrow\odot\rangle_3 \otimes \exp\left(i\frac{\pi}{8}\vec{a}\cdot\vec{S}_0\right) |S_0\uparrow\rangle \\ &= |\odot\uparrow\uparrow\uparrow\rangle_1 \otimes |\uparrow\uparrow\rangle_2 \otimes |\uparrow\uparrow\uparrow\odot\rangle_3 \otimes \left[ \cos\left(\frac{\pi}{8}\right) |S_0\uparrow\rangle + e^{i\frac{\pi}{4}} \sin\left(\frac{\pi}{8}\right) |S_0\downarrow\rangle \right]. \end{aligned} \quad (\text{A.23})$$

Similarly, when the ferromagnetic interval in the first chain is shifted away from the junction after this, the coupler undergoes another rotation  $\exp\left(i\frac{\pi}{8}\vec{b}\cdot\vec{S}_0\right)$  from the space diagonal  $\frac{1}{\sqrt{3}} \begin{pmatrix} 1 \\ 1 \\ 1 \end{pmatrix}$  about the axis  $\vec{b} = \frac{1}{\sqrt{2}} \begin{pmatrix} 0 \\ -1 \\ 1 \end{pmatrix}$  to the  $x$  direction  $\begin{pmatrix} 1 \\ 0 \\ 0 \end{pmatrix}$ . This results in the state

$$|\psi_3\rangle = e^{i\frac{\pi}{12}} |\uparrow\uparrow\uparrow\odot\rangle_1 \otimes |\uparrow\uparrow\rangle_2 \otimes |\uparrow\uparrow\uparrow\odot\rangle_3 \otimes \frac{1}{\sqrt{2}} \left[ |S_0\uparrow\rangle + |S_0\downarrow\rangle \right]. \quad (\text{A.24})$$

Retracting the remaining ferromagnetic interval is a trivial step again:

$$|\psi_4\rangle = e^{i\frac{\pi}{12}} |\uparrow\uparrow\uparrow\odot\rangle_1 \otimes |\odot\odot\rangle_2 \otimes |\odot\uparrow\uparrow\uparrow\rangle_3 \otimes \frac{1}{\sqrt{2}} \left[ |S_0\uparrow\rangle + |S_0\downarrow\rangle \right]. \quad (\text{A.25})$$

Unlike in the case of single-interval braiding (Sec. A.3), the coupler spin does not return to its initial state at the end of the operation.

For other initial conditions, the operation can be treated in a similar way, giving the complete result

$$|\blacklozenge\blacklozenge\circ\rangle_1 \otimes |\circ\blacklozenge\blacklozenge\rangle_3 \otimes |S_0 \uparrow\rangle \longrightarrow e^{i\frac{\pi}{12}} |\blacklozenge\blacklozenge\circ\rangle_1 \otimes |\circ\blacklozenge\blacklozenge\rangle_3 \otimes \frac{1}{\sqrt{2}} [ |S_0 \uparrow\rangle + |S_0 \downarrow\rangle ] \quad (\text{A.26a})$$

$$|\blacklozenge\blacklozenge\circ\rangle_1 \otimes |\circ\blacklozenge\blacklozenge\rangle_3 \otimes |S_0 \uparrow\rangle \longrightarrow e^{i\frac{\pi}{12}} |\blacklozenge\blacklozenge\circ\rangle_1 \otimes |\circ\blacklozenge\blacklozenge\rangle_3 \otimes \frac{1}{\sqrt{2}} [ |S_0 \uparrow\rangle - |S_0 \downarrow\rangle ] \quad (\text{A.26b})$$

$$|\blacklozenge\blacklozenge\circ\rangle_1 \otimes |\circ\blacklozenge\blacklozenge\rangle_3 \otimes |S_0 \downarrow\rangle \longrightarrow -e^{i\frac{\pi}{12}} |\blacklozenge\blacklozenge\circ\rangle_1 \otimes |\circ\blacklozenge\blacklozenge\rangle_3 \otimes \frac{1}{\sqrt{2}} [ |S_0 \uparrow\rangle - |S_0 \downarrow\rangle ] \quad (\text{A.26c})$$

$$|\blacklozenge\blacklozenge\circ\rangle_1 \otimes |\circ\blacklozenge\blacklozenge\rangle_3 \otimes |S_0 \downarrow\rangle \longrightarrow e^{i\frac{\pi}{12}} |\blacklozenge\blacklozenge\circ\rangle_1 \otimes |\circ\blacklozenge\blacklozenge\rangle_3 \otimes \frac{1}{\sqrt{2}} [ |S_0 \uparrow\rangle + |S_0 \downarrow\rangle ] \quad (\text{A.26d})$$

with placeholders  $\{\blacklozenge, \blacklozenge\} = \{\uparrow, \downarrow\}$ . The initial as well as final state of the second chain is always  $|\circ\circ\rangle_2$ . Using the parity eigenstates (A.20) for the two intervals, we can verify that Eqs. (A.26) indeed correspond to Majorana braiding, e. g. (neglecting the phase factor)

$$\begin{aligned} |0\rangle_1 \otimes |0\rangle_3 \otimes |S_0 \uparrow\rangle &= \frac{|\uparrow\uparrow\uparrow\rangle_1 + |\downarrow\downarrow\downarrow\rangle_1}{\sqrt{2}} \otimes \frac{|\uparrow\uparrow\uparrow\rangle_3 + |\downarrow\downarrow\downarrow\rangle_3}{\sqrt{2}} \otimes |S_0 \uparrow\rangle \\ &\longrightarrow \frac{|\uparrow\uparrow\uparrow\rangle_1 \otimes |\uparrow\uparrow\uparrow\rangle_3 + |\downarrow\downarrow\downarrow\rangle_1 \otimes |\downarrow\downarrow\downarrow\rangle_3}{2} \otimes \frac{|S_0 \uparrow\rangle + |S_0 \downarrow\rangle}{\sqrt{2}} \\ &\quad + \frac{|\uparrow\uparrow\uparrow\rangle_1 \otimes |\downarrow\downarrow\downarrow\rangle_3 + |\downarrow\downarrow\downarrow\rangle_1 \otimes |\uparrow\uparrow\uparrow\rangle_3}{2} \otimes \frac{|S_0 \uparrow\rangle - |S_0 \downarrow\rangle}{\sqrt{2}} \\ &= \frac{1}{\sqrt{2}} [ |0\rangle_1 \otimes |0\rangle_3 \otimes |S_0 \uparrow\rangle + |1\rangle_1 \otimes |1\rangle_3 \otimes |S_0 \downarrow\rangle ] . \end{aligned} \quad (\text{A.27})$$

In addition to the ferromagnetic intervals, the superposition involves the coupler spin, in accordance with the expression (2.16), which is compatible with the results (A.26).

Actually, the coupling  $J_{13}$  is unnecessary for the operation we considered here. The choice of  $J_{13} = 0$  simplifies the coupler rotations and leads to the same results only without the phase factor of  $\frac{\pi}{12}$ . [This geometric phase depends on the details of the coupler rotations (A.23), (A.25) and therefore cannot be described by the general expression (2.16).] Phase factors as well as symmetries which can be used to relax the requirement of ideal angle- $\frac{\pi}{2}$  spin rotations have been analysed in more detail for this two-interval spin equivalent of braiding in Refs. [34, 35].



# B

## Appendix B

# Effective action and phase fluctuations

For small charging energies, the dynamics of the Majorana island from Chap. 3 can be expressed conveniently in terms of the electromagnetic phase. An effective phase action for the system is derived in the first part of this appendix. The second part introduces the counting fields that are necessary to calculate transport quantities and explicates a decoupling of the phase action. In the third part, the decoupled action is used to evaluate phase-fluctuation averages in a low-energy limit.

## B.1 Derivation of the effective action

In order to describe the Majorana island and its coupling to the leads, we start from the assumption of a large superconducting gap  $\Delta$  on the island. The gap is assumed to be sufficiently large that the Majorana modes  $\gamma_j$ ,  $j \in \{\text{L}, \text{R}\}$ , with anti-commutation relation

$$\{\gamma_j, \gamma_k\} = \delta_{jk} , \quad (\text{B.1})$$

are the only fermionic degrees of freedom on the island. The electromagnetic phase  $\phi$  appears in the charging-energy term  $(\dot{\phi}^2/4E_c + n_0 \dot{\phi})$ , with gate charge  $q_0 = e n_0$ , as well as in the tunnel coupling to the leads. Following Ref. [22], we perform a gauge transformation that shifts the chemical potentials  $\mu_j$  of the leads to the tunneling terms. Using the dispersion relation  $\epsilon_{jk}$  and fermion fields  $\psi_{jk}$  for lead  $j$ , we obtain the fermionic part of the Lagrangian:

$$\mathcal{L}_f = \frac{1}{2} \sum_j \gamma_j i\partial_t \gamma_j + \sum_{jk} \bar{\psi}_{jk} (i\partial_t - \epsilon_{jk}) \psi_{jk} - \left( \sum_{jk} \lambda_j \bar{\psi}_{jk} e^{-i[\mu_j t + \phi(t)]} \gamma_j + \text{H. c.} \right) . \quad (\text{B.2})$$

For completeness, we briefly reiterate further derivation steps from Ref. [22]: To use the Keldysh formalism, we double all fields for the forward and backward branch. This leads to the new Lagrangian

$$\mathcal{L}_{ff} = \frac{1}{2} \sum_j \gamma_j^\top \tau_z i\partial_t \gamma_j + \sum_{jk} \bar{\psi}_{jk} \tau_z (i\partial_t - \epsilon_{jk}) \psi_{jk} - \left( \sum_{jk} \lambda_j \bar{\psi}_{jk} \tau_z e^{-i[\mu_j t + \check{\phi}(t)]} \gamma_j + \text{H. c.} \right) , \quad (\text{B.3})$$

where the phase is expressed as a matrix  $\check{\phi} = \text{diag}(\phi^+, \phi^-)$ , or  $\check{\phi} = \phi_c + \tau_z \phi_q$  in terms of the classical and quantum Keldysh components,  $\tau_i$  are Pauli matrices in Keldysh space and the fermion fields are now vectors, e. g.  $\gamma_j^\top = (\gamma_j^+, \gamma_j^-)$ .

The chemical potential of the Majorana island,  $\mu_M = \langle \dot{\phi}_c \rangle$ , is determined by current conservation and fixes the average time derivative of the classical phase component  $\phi_c$ . We can separate this time dependence from  $\phi_c$ , which then contains only the fluctuations of the phase around the mean-field value ( $\mu_M t$ ). To compensate the resulting changes in the Lagrangian, we renormalise the gate charge  $q_0$  and both lead chemical potentials, which are thereby transformed into the voltages at the contacts to the leads,  $\mu_j \rightarrow V_j$ . After that, integrating out the lead fermions  $\psi_{jk}$  in a wide-band approximation and using the Keldysh rotation

$$\check{L} = \frac{1}{\sqrt{2}} \begin{pmatrix} 1 & -1 \\ 1 & 1 \end{pmatrix} \quad (\text{B.4})$$

for the Majorana operators,  $\tilde{\gamma}_j = \check{L} \gamma_j$ , yields an effective action [22]

$$S_{\text{eff}} = \frac{1}{2} \sum_j \int dt dt' \tilde{\gamma}_j^T \left[ \tau_x i \partial_t \delta(t-t') + \check{Q}_j(t, t') \right] \tilde{\gamma}_j, \quad (\text{B.5})$$

$$\check{Q}_j(t, t') = i \Gamma_j e^{i \tau_x \phi_q(t)/2} \begin{pmatrix} \delta_-(t-t') & 2F(t-t') e^{i \Phi_j(t, t')} \\ 0 & -\delta_+(t-t') \end{pmatrix} \tau_x e^{-i \tau_x \phi_q(t')/2}. \quad (\text{B.6})$$

Here,  $F$  is the thermal distribution function for both leads, the coupling  $\Gamma_j = 2\pi \nu_j |\lambda_j|^2$  contains the density of states  $\nu_j = \sum_k \delta(\epsilon_{jk})$  in the corresponding lead, the functions  $\delta_{\pm}(t) \equiv \delta(t \pm 0^+)$  include infinitesimal shifts to ensure proper causality, and the quantities  $\Phi_j$  are defined in Eq. (3.6). Integration over the Majorana fields results in the fermionic action [22]

$$iS_f = \frac{1}{2} \sum_j \text{Tr} \ln \left[ \tau_x i \partial_t \delta(t-t') + \check{A}_j(t, t') \right], \quad (\text{B.7})$$

$$\check{A}_j(t, t') = \frac{1}{2} \left[ \check{Q}_j(t, t') - \check{Q}_j^T(t', t) \right]. \quad (\text{B.8})$$

All Keldysh components of the Majorana Green's function

$$\check{G}_j = \begin{pmatrix} 0 & G_j^A \\ G_j^R & G_j^K \end{pmatrix} \quad (\text{B.9})$$

are defined using the classical part of  $\check{A}_j$  only:

$$\check{G}_j^{-1}(t, t') = \left[ \tau_x i \partial_t \delta(t-t') + \check{A}_j(t, t') \right]_{\phi_q=0}. \quad (\text{B.10})$$

Expansion of  $S_f$  to second order in the quantum phase  $\phi_q$  then yields the expression (3.3).

## B.2 Fluctuation kernel and decoupling

This appendix contains full expressions for the quantum fluctuation of the effective action and their Hubbard–Stratonovich decoupling (Sec. 3.3), including the counting fields  $\chi_L, \chi_R$  used to calculate the currents at both contacts and their correlations. They appear alongside  $\phi_q$  in the action terms

originating from the coupling to the leads:

$$iS_f[\chi_L, \chi_R] = i \sum_j \int dt \mathcal{I}_j(t) [\phi_q(t) + \chi_j(t)] - \frac{1}{2} \sum_j \int dt dt' [\phi_q(t) + \chi_j(t)] K_j(t-t') [\phi_q(t') + \chi_j(t')] . \quad (\text{B.11})$$

Like the current operator  $\mathcal{I}(t)$ , the fluctuation kernel  $K(t-t') = \sum_j K_j(t-t')$  with  $j \in \{\text{L}, \text{R}\}$ , consists of contributions from the left and right contact [22]. The complete expressions also depend on the classical phase component  $\phi_c$ :

$$K_j(t, t') = \frac{1}{2} \Gamma_j \delta(t-t') - \Gamma_j^2 \int dt_1 dt_2 G_j^R(t-t_1) G_j^R(t'-t_2) \cdot [F(t-t') \cos \Phi_j(t, t') F(t_1-t_2) \cos \Phi_j(t_1, t_2) + F(t_1-t') \sin \Phi_j(t_1, t') F(t_2-t) \sin \Phi_j(t_2, t)] . \quad (\text{B.12})$$

As phase fluctuations are strongly suppressed for a small charging energy  $E_c$ , we neglect the  $\phi_c$  dependence of  $K$ ,

$$K_j(t, t') \approx K_j(t, t')|_{\phi_c=0} = K_j(t-t') , \quad (\text{B.13})$$

in the rest of our calculations. Then, we can easily decouple the  $\phi_q$ -quadratic part of the action:

$$\prod_j \exp \left[ -\frac{1}{2} \int dt dt' [\phi_q(t) + \chi_j(t)] K_j(t-t') [\phi_q(t') + \chi_j(t')] \right] = \int \mathcal{D}[\xi_L, \xi_R] \prod_j \exp \left[ -\frac{1}{2} \int dt dt' \xi_j(t) K_j^{-1}(t-t') \xi_j(t') + i \int dt [\phi_q(t) + \chi_j(t)] \xi_j(t) \right] . \quad (\text{B.14})$$

### B.3 Low-energy evaluation of noise averages

In the low energy limit  $\omega \ll \Gamma_j$ , the Langevin equation (3.9) can be simplified by approximating the dampening kernel  $\eta$  with its zero-frequency value,

$$\eta(t-t') \approx \eta_0 \delta(t-t') , \quad (\text{B.15})$$

which is calculated in Ref. [22] for both finite temperature and  $T = 0$ :

$$\eta_0 = \frac{2}{\pi} \sum_j \int \frac{d\epsilon}{4T} \frac{1}{\cosh^2\left(\frac{\epsilon}{2T}\right)} \left[ \left( \frac{\epsilon - V_j}{\Gamma_j} \right)^2 + 1 \right]^{-1} \quad (\text{B.16})$$

$$\xrightarrow{T \rightarrow 0} \frac{2}{\pi} \sum_j \frac{1}{(V_j/\Gamma_j)^2 + 1} . \quad (\text{B.17})$$

For the Langevin equation in the time domain, this yields

$$2 E_c \sum_j \xi_j(t) \approx \ddot{\phi}_c + \Omega \dot{\phi}_c(t) , \quad (\text{B.18})$$

with the inverse *RC* time given by  $\Omega = \eta_0 E_c$ . The retarded propagator  $D^R$  takes on the form [22]:

$$D^R(t) \approx \frac{1 - e^{-\Omega t}}{\eta_0} \Theta(t) \iff \eta_0 D^R(\omega) \approx \frac{i}{\omega} - \frac{1}{\Omega - i\omega} + \pi \delta(\omega) . \quad (\text{B.19})$$

To calculate the currents and their correlation, we have to evaluate some noise averages of the fluctuation fields  $\xi_j$  and the classical phase  $\bar{\phi}_c$ . Using the relations (3.8) and (3.10), we easily obtain an expression for a phase–phase average:

$$\begin{aligned} \langle \bar{\phi}_c(t) \bar{\phi}_c(t') \rangle_\xi &= \int d\tau d\tau' D^R(t - \tau) \sum_j \langle \xi_j(\tau) \xi_j(\tau') \rangle D^R(t' - \tau') \\ &= \int d\tau d\tau' D^R(t - \tau) K(\tau - \tau') D^R(t' - \tau') . \end{aligned} \quad (\text{B.20})$$

For this calculation, it is convenient to define the quantity [22]

$$\begin{aligned} J(t) &= \frac{1}{2} \langle [\bar{\phi}_c(t) - \bar{\phi}_c(0)]^2 \rangle_\xi = \langle -[\bar{\phi}_c(t) - \bar{\phi}_c(0)] \bar{\phi}_c(0) \rangle_\xi \\ &= \frac{1}{\eta_0^2} \int \frac{d\omega}{2\pi} K(\omega) \frac{1 - \cos(\omega t)}{\omega^2 (1 + \omega^2/\Omega^2)} = J(-t) . \end{aligned} \quad (\text{B.21})$$

( $K$  is symmetrical.) Similarly, a mixed average of  $\bar{\phi}_c$  and  $\xi_k$  is given by

$$\begin{aligned} \langle \bar{\phi}_c(t) \xi_k(t') \rangle_\xi &= \int d\tau D^R(t - \tau) \langle \xi_k(\tau) \xi_k(t') \rangle = \int d\tau D^R(t - \tau) K_k(\tau - t') \\ &= \int \frac{d\omega}{2\pi} D^R(\omega) K_k(\omega) e^{-i\omega(t-t')} . \end{aligned} \quad (\text{B.22})$$

# C Details of the correlation calculation

Charging energy on a Majorana island can mediate current correlations between different contacts (Chap. 3). The first part of this appendix contains the derivation of analytical expressions for the correlation at large coupling  $\Gamma$ . Further approximations in the limit of zero temperature are detailed in the second part.

## C.1 Current and correlation in the limit of large $\Gamma$

Starting from the assumptions (3.17) in Sec. 3.5, we will omit any corrections beyond the leading order in  $\Gamma_j^{-1}$ . Both  $J(t)$  and the distribution function  $F(t)$  have the same time argument as the exponential decay of  $G_j^R(t)$  in the current [22]

$$I_j(t) = \langle \mathcal{I}_j(t) \rangle_\xi = \Gamma_j \int dt' F(t' - t) \sin[V_j(t' - t)] G_j^R(t - t') e^{-J(t-t')} . \quad (\text{C.1})$$

Therefore, we neglect the function  $J(t)$ , which is continuous with  $J(0) = 0$ , at this point and approximate  $F(t)$  by its zero-temperature limit,

$$F(t) = \frac{-i T}{\sinh(\pi T t)} \approx -\frac{i}{\pi t} = F_0(t) , \quad (\text{C.2})$$

to obtain the following result for the current:

$$I_j(t) \approx \Gamma_j \int d\tau F_0(\tau) \sin(V_j \tau) G_j^R(-\tau) = -\frac{\Gamma_j}{\pi} \arctan\left(\frac{V_j}{\Gamma_j}\right) \approx -\frac{V_j}{\pi} . \quad (\text{C.3})$$

The correlation expressions can be treated in a similar way. By symmetry, in the term

$$\mathcal{I}_j(t_j) \xi_k(t_k) = \Gamma_j \int dt' F(t' - t) \sin\Phi_j(t', t) G_j^R(t - t') \xi_k(t_k) \quad (\text{C.4})$$

(unlike for the current), the second contribution from the angle addition formula,

$$\sin\Phi_j(t', t) = \sin[V_j(t' - t)] \cos[\bar{\phi}_c(t') - \bar{\phi}_c(t)] + \cos[V_j(t' - t)] \sin[\bar{\phi}_c(t') - \bar{\phi}_c(t)] , \quad (\text{C.5})$$

yields a finite expectation value:

$$\begin{aligned}
\langle \mathcal{I}_j(t_j) \xi_k(t_k) \rangle_\xi &= \Gamma_j \int d\tau F(\tau) \cos(V_j \tau) G_j^{\text{R}}(-\tau) \left\langle \sin[\bar{\phi}_c(t_j + \tau) - \bar{\phi}_c(t_j)] \xi_k(t_k) \right\rangle_\xi \\
&= \Gamma_j \int dt' F(\tau) \cos(V_j \tau) G_j^{\text{R}}(-\tau) e^{-J(\tau)} \left\langle [\bar{\phi}_c(t_j + \tau) - \bar{\phi}_c(t_j)] \xi_k(t_k) \right\rangle_\xi \\
&\approx \Gamma_j \int dt' F_0(\tau) \cos(V_j \tau) G_j^{\text{R}}(-\tau) \left\langle [\bar{\phi}_c(t_j + \tau) - \bar{\phi}_c(t_j)] \xi_k(t_k) \right\rangle_\xi \\
&\stackrel{(3.10)}{=} \Gamma_j \int d\tau F_0(\tau) \cos(V_j \tau) G_j^{\text{R}}(-\tau) \int d\tau' [D^{\text{R}}(t + \tau - \tau') - D^{\text{R}}(t - \tau')] K_k(\tau' - t_k) \\
&= \Gamma_j \int d\tau F_0(\tau) \cos(V_j \tau) G_j^{\text{R}}(-\tau) \int \frac{d\omega}{2\pi} D^{\text{R}}(\omega) K_k(\omega) [e^{-i\omega\tau} - 1] e^{-i\omega(t-t_k)} \\
&= -\frac{\Gamma_j}{2\pi} \int \frac{d\omega}{2\pi} e^{-i\omega(t-t_k)} D^{\text{R}}(\omega) K_k(\omega) \ln \left[ \frac{V_j^2 + (\Gamma_j - i\omega)^2}{V_j^2 + \Gamma_j^2} \right]. \tag{C.6}
\end{aligned}$$

Both  $J(t)$  and the finite temperature in  $F(t)$  have, again, been neglected for small time arguments  $t = \tau \lesssim \Gamma_j^{-1}$ . Additionally, the Fourier transform can be expanded in the small voltage  $V_j$  and frequency  $\omega$ :

$$-\frac{\Gamma_j}{2\pi} D^{\text{R}}(\omega) K_k(\omega) \ln \left[ \frac{V_j^2 + (\Gamma_j - i\omega)^2}{V_j^2 + \Gamma_j^2} \right] \approx -\frac{1}{4} \left[ 1 + i\omega \left( \frac{1}{\Omega} + \frac{1}{2\Gamma_j} \right) - \frac{\omega^2}{2\Gamma_j\Omega} \right] \frac{\Omega^2}{\omega^2 + \Omega^2} K_k(\omega). \tag{C.7}$$

In both factors of the last term,  $\mathcal{I}_L(t_L) \mathcal{I}_R(t_R)$ , the angle addition formula (C.5) can be used, yielding two non-vanishing contributions:

$$\begin{aligned}
&2 \left\langle \frac{\cos}{\sin} [\bar{\phi}_c(t'_L) - \bar{\phi}_c(t_L)] \cdot \frac{\cos}{\sin} [\bar{\phi}_c(t'_R) - \bar{\phi}_c(t_R)] \right\rangle_\xi \\
&= \exp \left[ -\frac{1}{2} \left\langle [\bar{\phi}_c(t'_L) - \bar{\phi}_c(t_L) - \bar{\phi}_c(t'_R) + \bar{\phi}_c(t_R)]^2 \right\rangle_\xi \right] \\
&\quad \pm \exp \left[ -\frac{1}{2} \left\langle [\bar{\phi}_c(t'_L) - \bar{\phi}_c(t_L) + \bar{\phi}_c(t'_R) - \bar{\phi}_c(t_R)]^2 \right\rangle_\xi \right] \\
&= 2 e^{-[J(t_L - t'_L) + J(t_R - t'_R)]} \cdot \frac{\cosh}{\sinh} \left[ \left\langle [\bar{\phi}_c(t'_L) - \bar{\phi}_c(t_L)] [\bar{\phi}_c(t'_R) - \bar{\phi}_c(t_R)] \right\rangle_\xi \right] \\
&= 2 e^{-J(t_L - t'_L)} \cdot e^{-J(t_R - t'_R)} \cdot \frac{\cosh}{\sinh} [J(t_L - t'_R) + J(t'_L - t_R) - J(t'_L - t'_R) - J(t_L - t_R)]. \tag{C.8}
\end{aligned}$$

Obtaining the leading contributions is slightly more complex, here. The prefactor exponentials can be neglected, as  $J(t)$  appears with a small argument there. Using  $t \equiv t_L - t_R$  in the expression

$$\begin{aligned}
\langle \mathcal{I}_L(t_L) \mathcal{I}_R(t_R) \rangle_\xi &\approx \Gamma_L \int d\tau_L F(\tau_L) G_j^{\text{R}}(-\tau_L) \cdot \Gamma_R \int d\tau_R F(\tau_R) G_j^{\text{R}}(-\tau_R) \\
&\quad \cdot \left\{ \sin(V_L \tau_L) \sin(V_R \tau_R) \cosh [J(t - \tau_R) + J(t + \tau_L) - J(t + \tau_L - \tau_R) - J(t)] \right. \\
&\quad \left. + \cos(V_L \tau_L) \cos(V_R \tau_R) \sinh [J(t - \tau_R) + J(t + \tau_L) - J(t + \tau_L - \tau_R) - J(t)] \right\}, \tag{C.9}
\end{aligned}$$

we expand the (hyperbolic) sine and cosine functions in the small parameters  $\tau_j$ . The constant part of the cosh expansion cancels with the term  $I_L(t_L) I_R(t_R)$ :

$$\begin{aligned} \langle \mathcal{I}_L(t_L) \mathcal{I}_R(t_R) \rangle_\xi - I_L(t_L) I_R(t_R) &\approx \Gamma_L \int d\tau_L F_0(\tau_L) G_j^R(-\tau_L) \cdot \Gamma_R \int d\tau_R F_0(\tau_R) G_j^R(-\tau_R) \\ &\quad \cdot \left[ \tau_L \tau_R J''(t) + \frac{\tau_L^2 \tau_R - \tau_L \tau_R^2}{2} J^{(3)}(t) \right] \\ &= \frac{1}{\pi^2} J''(t) + \frac{1}{2\pi^2} \left( \frac{1}{\Gamma_R} - \frac{1}{\Gamma_L} \right) J^{(3)}(t) . \end{aligned} \quad (\text{C.10})$$

By inserting the quantity  $\eta_0 \approx \frac{4}{\pi}$  into the definition (B.21) of  $J$ ,

$$\Rightarrow J''(t) = \frac{1}{\eta_0^2} \int \frac{d\omega}{2\pi} K(\omega) \frac{\cos(\omega t)}{1 + \omega^2/\Omega^2} \approx \int \frac{d\omega}{2\pi} \cos(\omega t) \frac{\pi^2}{16} \frac{\Omega^2}{\omega^2 + \Omega^2} K(\omega) , \quad (\text{C.11})$$

we obtain simple expressions for the Fourier transform of the terms in Eq. (C.10):

$$\frac{1}{\pi^2} J''(t) + \frac{1}{2\pi^2} \left( \frac{1}{\Gamma_R} - \frac{1}{\Gamma_L} \right) J^{(3)}(t) \quad \longrightarrow \quad \frac{1}{16} \left[ 1 - \frac{i\omega}{2} \left( \frac{1}{\Gamma_R} - \frac{1}{\Gamma_L} \right) \right] \frac{\Omega^2}{\omega^2 + \Omega^2} K(\omega) . \quad (\text{C.12})$$

Combining the results of the  $\mathcal{I}_L(t_L) \mathcal{I}_R(t_R)$  term, Eq. (C.12), and of both  $\mathcal{I}_j(t_j) \xi_k(t_k)$  terms, given in Eq. (C.7), we arrive at the correlation function

$$\begin{aligned} C_{LR}(\omega) &\approx -\frac{1}{4} \left[ 1 + i\omega \left( \frac{1}{\Omega} + \frac{1}{2\Gamma_L} \right) - \frac{\omega^2}{2\Gamma_L \Omega} \right] \frac{\Omega^2}{\omega^2 + \Omega^2} K_R(\omega) \\ &\quad - \frac{1}{4} \left[ 1 - i\omega \left( \frac{1}{\Omega} + \frac{1}{2\Gamma_R} \right) - \frac{\omega^2}{2\Gamma_R \Omega} \right] \frac{\Omega^2}{\omega^2 + \Omega^2} K_L(\omega) \\ &\quad + \frac{1}{16} \left[ 1 + \frac{i\omega}{2} \left( \frac{1}{\Gamma_L} - \frac{1}{\Gamma_R} \right) \right] \frac{\Omega^2}{\omega^2 + \Omega^2} K(\omega) . \end{aligned} \quad (\text{C.13})$$

In the symmetrised correlator, the imaginary part obviously vanishes. Taking into account the leading-order contributions to the real part only, we obtain the expression (3.18).

## C.2 Further treatment of the zero-temperature case

At  $T = 0$ , the fluctuation kernels are given by [22]

$$K_j(\omega) = \sum_{\pm} \frac{\Gamma_j}{2\pi} \tan^{-1} \left( \frac{\omega \pm V_j}{\Gamma_j} \right) + K_j^V(\omega) \approx K_j^0(\omega) + K_j^V(\omega) , \quad (\text{C.14})$$

$$\begin{aligned} K_j^V(\omega) &= \frac{\Gamma_j}{2\pi} \Theta(2|V_j| - |\omega|) \\ &\quad \cdot \left[ \tan^{-1} \left( \frac{|V_j|}{\Gamma_j} \right) + \tan^{-1} \left( \frac{|V_j| - |\omega|}{\Gamma_j} \right) + \frac{\Gamma_j}{|\omega|} \ln \left( \frac{(|V_j| - |\omega|)^2 + \Gamma_j^2}{V_j^2 + \Gamma_j^2} \right) \right] . \end{aligned} \quad (\text{C.15})$$

We can use a linear spectrum for the first, leading contribution,

$$K_j^0(\omega) = \frac{|\omega|}{\pi}, \quad (\text{C.16})$$

to compute an approximation for the function  $J''$  (C.11):

$$J_0''(t) = -\frac{\Omega^2}{16} \left[ e^{\Omega t} \text{Ei}(-\Omega t) + e^{-\Omega t} \text{Ei}(\Omega t) \right], \quad (\text{C.17})$$

where  $\text{Ei}(x) = -\int_{-x}^{\infty} \frac{dx}{x} e^{-x}$  is an exponential integral.

The sin–sin–cosh term in Eq. (C.9) vanishes in equilibrium. Otherwise, the lowest-order expansion in the small times  $\tau_j$  yields

$$\begin{aligned} & \Gamma_L \int d\tau_L F(\tau_L) G_j^R(-\tau_L) \cdot \Gamma_R \int d\tau_R F(\tau_R) G_j^R(-\tau_R) V_L \tau_L V_R \tau_R \frac{\tau_L^2 \tau_R^2}{2} J''(t)^2 \\ &= \frac{2 V_L V_R}{\pi^2 \Gamma_L^2 \Gamma_R^2} J''(t)^2. \end{aligned} \quad (\text{C.18})$$

By using the approximation  $J''(t) \approx J_0''(t)$  and applying the Fourier transformation,

$$\xrightarrow{\text{FT}} \frac{V_L V_R}{\Gamma_L^2 \Gamma_R^2} \frac{\Omega^4}{32\pi} \frac{\pi \Omega - 2 \Omega \arctan\left(\frac{|\omega|}{\Omega}\right) + |\omega| \left(1 + 2\frac{\Omega^2}{\omega^2}\right) \ln\left(1 + \frac{\omega^2}{\Omega^2}\right)}{\omega^2 + 4 \Omega^2} \xrightarrow{\omega=0} \frac{\Omega^3 V_L V_R}{128 \Gamma_L^2 \Gamma_R^2}, \quad (\text{C.19})$$

we obtain an additional contribution relevant for small frequencies.

# D Supercurrent in a thermal state

The Josephson current in a system containing two superconductors can be determined from a quantum-mechanical partition function with a dependence on the superconducting phase difference  $\chi$ . Starting from the partition function for the canonical or grand-canonical ensemble, quite general expressions for the thermal supercurrent, which are useful for the calculations in App. E and Chap. 4, are derived in this appendix.

Phase and charge are conjugate observables. Therefore the Josephson current  $\mathcal{I}_J$  in a junction of two superconductors can be calculated from the (grand-)canonical partition function for the Hamiltonian  $H$ ,

$$\mathcal{Z} = \text{Tr} \left[ e^{-\beta H} \right] = \sum_n e^{-\beta E_n} , \quad (\text{D.1})$$

where  $\beta = (k_B T)^{-1}$  gives the temperature scale and the eigenvalues of  $H$  are

$$E_n = \langle n | H | n \rangle , \quad (\text{D.2})$$

as a derivative of the thermodynamic potential

$$F = -\beta^{-1} \ln(\mathcal{Z}) \quad (\text{D.3})$$

with respect to the phase difference  $\chi$ :

$$\mathcal{I}_J = \frac{2e}{\hbar} \frac{\partial F}{\partial \chi} = \frac{2e}{\hbar \mathcal{Z}} \sum_n \frac{\partial E_n}{\partial \chi} e^{-\beta E_n} . \quad (\text{D.4})$$

Given the expression for the Hamiltonian  $H = \sum_n |n\rangle E_n \langle n|$ , it easily follows that for any energy eigenstate  $|n\rangle$ , we can use the derivative of the expectation value and the expectation value of the derivative interchangeably:

$$\Rightarrow \frac{\partial E_n}{\partial \chi} = \frac{\hbar}{2e} \langle n | I_J | n \rangle \quad \text{for} \quad I_J = \frac{2e}{\hbar} \frac{\partial H}{\partial \chi} . \quad (\text{D.5})$$

Hence, the current is given by

$$\mathcal{I}_J = \mathcal{Z}^{-1} \sum_n \langle n | I_J e^{-\beta H} | n \rangle = \mathcal{Z}^{-1} \text{Tr} \left[ I_J e^{-\beta H} \right] . \quad (\text{D.6})$$

Discrete sums over eigenstates  $|n\rangle$  are not well suited to the limit of a continuous spectrum. Therefore, it can be useful to introduce the density of states  $\rho(\epsilon) = \sum_n \delta(E_n - \epsilon)$ , which becomes a continuous function in this limit. There are two possibilities to introduce  $\rho$  in the current calculation: If we start from the expression

$$\mathcal{Z} = \int d\epsilon \rho(\epsilon) e^{-\beta \epsilon} \quad (\text{D.7})$$

for the partition function, only  $\rho$  has a phase dependence (via the eigenenergies  $E_n$ ), so the current is given by

$$\mathcal{I}_J = -\frac{2e}{\hbar \beta \mathcal{Z}} \int d\epsilon \frac{\partial \rho(\epsilon)}{\partial \chi} e^{-\beta \epsilon} . \quad (\text{D.8})$$

The alternative is carrying out the phase derivative first, which yields Eq. (D.4). If the current contribution per state is a function of energy,

$$I(E_n) = \frac{2e}{\hbar} \frac{\partial E_n}{\partial \chi} , \quad (\text{D.9})$$

we can express the total current via the density of states in a different way:

$$\mathcal{I}_J = \mathcal{Z}^{-1} \int d\epsilon \rho(\epsilon) I(\epsilon) e^{-\beta \epsilon} . \quad (\text{D.10})$$

From a simple comparison between equations (D.8) and (D.10), it follows that the current contribution at energy  $\epsilon$  is, in fact, given by

$$I(\epsilon) = -\frac{2e}{\hbar \beta \rho} \frac{\partial \rho}{\partial \chi} , \quad (\text{D.11})$$

which is a function of energy (with parameter  $\chi$ ).

Note that, in general, the density of states  $\rho$  consists of both extensive and subextensive contributions. For a two-dimensional system of area  $L^2$ , e. g., it can be written

$$\rho = \rho_0 + \rho_1 L + \rho_2 L^2 . \quad (\text{D.12})$$

in the limit  $L \rightarrow \infty$ . Like the distance of energy levels, the quantity  $I(\epsilon)$  scales as  $1/L$ . From the relation (D.11), we conclude that only *subextensive* contributions to the density of states can depend on the phase  $\chi$ . Both the product  $L^2 \rho_2(\epsilon) I(\epsilon)$  involving the extensive part of  $\rho$  in Eq. (D.10) for the second approach and the derivative of a subextensive part,  $L \partial \rho_1 / \partial \chi$ , in the first approach (D.8) scale linear in  $L$ , yielding the leading contribution to the current  $\mathcal{I}_J$ . A more detailed analysis has been carried out for similar scaling behaviour of flux-dependent persistent currents in Ref. [36].

# E

## Appendix E

# Current calculation via eigenmodes

The current–phase relation of a Josephson junction can be determined from the dependence of the eigenenergies of the Hamiltonian on the superconducting phase difference (cf. App. D). However, this dependence can be rather difficult to determine in a system with a continuous spectrum. In this appendix, the supercurrent contribution for any eigenmode of the topological Josephson contact from Chap. 4 will be expressed in terms of the particular wave function, instead.

In the following, we will derive the supercurrent contribution for an excitation with a 4-component spinor wavefunction  $\Xi = [\xi_1, \xi_2, \xi_3, \xi_4]^T$ , created by

$$\alpha^\dagger = \int dx dy \Psi^\dagger(x, y) \Xi(x, y) . \quad (\text{E.1})$$

The Hamiltonian (4.1) has the diagonal form

$$H = E_0 - \frac{1}{2} \sum_j \epsilon_j + \sum_j \epsilon_j \alpha_j^\dagger \alpha_j \quad (\text{E.2})$$

with eigenmodes  $\alpha_j$ . (For the continuous part of the spectrum, the sums are to be taken as integrals, of course.)

Due to the particle–hole doubling in the initial expression for the Hamiltonian, an additional sum over the energies of all eigenmodes appears here. That is why excitations are relevant even for the zero-temperature supercurrent. As we have already derived the scattering modes and bound states of the system, we can restrict our calculation to these wavefunctions. For a bound state, we can determine the current contribution directly from the phase dependence of the energy  $\epsilon$  (cf. App. D):

$$I_\alpha = \frac{2e}{\hbar} \frac{\partial \epsilon}{\partial \chi} . \quad (\text{E.3})$$

In the following, we will show that the current contribution for an arbitrary eigenmode  $\alpha$  is given by

$$I_\alpha = e v \int dy \left[ \xi_1^* \xi_2 + \xi_2^* \xi_1 + \xi_3^* \xi_4 + \xi_4^* \xi_3 \right]_{x=0} , \quad (\text{E.4})$$

which is, for scattering states (and bound states in the SNS case), identical to the expression

$$I_\alpha = \frac{e v^2 k_M}{\epsilon} \int dy \left( |A_{(e)}^+|^2 - |A_{(e)}^-|^2 - |A_{(h)}^+|^2 + |A_{(h)}^-|^2 \right) \quad (\text{E.5})$$

in terms of the momentum  $k_M$ , the energy  $\epsilon$  and the coefficients  $A$  of the eigenfunctions (4.4).

First, we apply a gauge transformation by redefining the fermionic operators,

$$\begin{bmatrix} \psi_\uparrow \\ \psi_\downarrow \\ +\psi_\downarrow^\dagger \\ -\psi_\uparrow^\dagger \end{bmatrix} \longrightarrow \begin{bmatrix} e^{-i\varphi(x)/2} \psi_\uparrow \\ e^{-i\varphi(x)/2} \psi_\downarrow \\ +e^{i\varphi(x)/2} \psi_\downarrow^\dagger \\ -e^{i\varphi(x)/2} \psi_\uparrow^\dagger \end{bmatrix}, \quad (\text{E.6})$$

in order to shift the phase dependence in the Hamiltonian from the order parameters in the superconducting areas to the middle region. The phase  $\varphi$  depends on the coordinate  $x$ ; it has to satisfy  $\varphi(x) = \phi_L$  for  $x < -B/2$  and  $\varphi(x) = \phi_R$  for  $x > B/2$ . In the middle region, the choice of gauge is not important and does not need to be fixed yet.

A gauge transformation generally involves a change of the wavefunctions. However, the expression (E.4) mixes components only within the particle or the hole block, so the phase shift  $\varphi$  in the wavefunction cancels out and can be ignored in this calculation. The only phase dependence remaining in the transformed Hamiltonian,

$$h \rightarrow v \vec{p} \cdot \vec{\sigma} \tau_z + M(x) \sigma_z + |\Delta(x)| \tau_x - \frac{\hbar v}{2} \sigma_x \frac{\partial \varphi(x)}{\partial x}, \quad (\text{E.7})$$

comes from the gauge transformation itself. Therefore the current operator, defined in App. D by Eq. (D.5), takes on the convenient form

$$\begin{aligned} I_J &= -\frac{ev}{2} \int dx dy \frac{\partial^2 \varphi(x)}{\partial \chi \partial x} \Psi^\dagger \sigma_x \Psi \\ &= -ev \int dx dy \frac{\partial^2 \varphi(x)}{\partial \chi \partial x} \left[ \psi_\uparrow^\dagger \psi_\downarrow + \psi_\downarrow^\dagger \psi_\uparrow \right]. \end{aligned} \quad (\text{E.8})$$

Starting from the superconducting ground state  $|\Omega\rangle$ , we calculate the current contribution  $I_\alpha$ , using the relations  $\alpha \alpha^\dagger |\Omega\rangle = |\Omega\rangle$  and  $\alpha |\Omega\rangle = 0$  as well as a bit of (anti-)commutation algebra:

$$\begin{aligned} I_\alpha &= \langle \Omega | \alpha I_J \alpha^\dagger | \Omega \rangle - \langle \Omega | I_J | \Omega \rangle \\ &= \langle \Omega | \alpha [I_J, \alpha^\dagger] | \Omega \rangle \\ &= \langle \Omega | \left\{ \alpha, [I_J, \alpha^\dagger] \right\} | \Omega \rangle. \end{aligned} \quad (\text{E.9})$$

With the usual fermionic anti-commutation relation  $\{\psi_\mu(\vec{r}), \psi_\nu^\dagger(\vec{s})\} = \delta_{\mu\nu} \delta(\vec{r}-\vec{s})$ , both the commutator and the anti-commutator can easily be determined:

$$C_\alpha = [I_J, \alpha^\dagger] = -ev \int dx dy \frac{\partial^2 \varphi(x)}{\partial \chi \partial x} \left[ \psi_\uparrow^\dagger \xi_2 + \psi_\downarrow^\dagger \xi_1 + \psi_\downarrow \xi_4 - \psi_\uparrow \xi_3 \right] \quad (\text{E.10})$$

$$\Rightarrow \{\alpha, C_\alpha\} = -ev \int dx dy \frac{\partial^2 \varphi(x)}{\partial \chi \partial x} \left[ \xi_1^* \xi_2 + \xi_2^* \xi_1 + \xi_3^* \xi_4 + \xi_4^* \xi_3 \right]. \quad (\text{E.11})$$

---

What remains to be fixed is the gauge in the region between the superconductors. As, in fact, the rest of the integrand does not depend on position in the interval  $-B/2 \leq x \leq B/2$ , it does not matter how exactly  $\varphi$  is defined there. A simple choice is a jump at  $x = 0$ ,

$$\frac{\partial\varphi(x)}{\partial x} = - \underbrace{(\phi_L - \phi_R)}_{\chi} \delta(x) \quad (\text{E.12})$$

$$\Rightarrow \frac{\partial^2\varphi(x)}{\partial\chi\partial x} = -\delta(x) , \quad (\text{E.13})$$

yielding the expression (E.4).

Now we can use the relations (D.4) and (D.5) as well as the diagonal Hamilton (E.2) to determine the total Josephson current for an arbitrary temperature ( $k_B T = \beta^{-1}$ ):

$$\begin{aligned} \mathcal{I}_J &= -\frac{1}{2} \sum_j I_{\alpha_j} + \sum_j I_{\alpha_j} \langle \alpha_j^\dagger \alpha_j \rangle \\ &= -\frac{1}{2} \sum_j I_{\alpha_j} \tanh\left(\frac{\beta \epsilon_j}{2}\right) , \end{aligned} \quad (\text{E.14})$$

where  $\langle \dots \rangle$  is the thermal expectation value, yielding a Fermi distribution.



# List of Figures

1.1	Majorana pairings in the Kitaev chain (diagram inspired by Ref. [2]) . . . . .	4
1.2	Topological and non-topological order . . . . .	4
1.3	Schematic picture of a topological wire (inspired by Ref. [6]) . . . . .	4
1.4	World-line diagram of a braiding operation (inspired by Ref. [8]) . . . . .	5
1.5	Majorana braiding in a T junction (picture inspired by Ref. [6]) . . . . .	6
2.1	Binary-tree structure of fermionic or spin chains . . . . .	10
4.1	Josephson junction on a TI surface . . . . .	22
4.2	Bound-state masses in the SNS case . . . . .	25
4.3	Signed bound-state masses in the SNS case . . . . .	25
4.4	Bound-state mass in the SMS case . . . . .	28
4.5	Comparison of current–phase relations . . . . .	31
4.6	Quantity characterising the shape of the current–phase relation . . . . .	31
4.7	Josephson current as a function of junction width . . . . .	32
4.8	Logarithmic plots showing the decay of Josephson current . . . . .	32
A.1	Ising spin chains in a T geometry . . . . .	38



# Bibliography

- <sup>1</sup>D. A. Ivanov, „Non-Abelian statistics of half-quantum vortices in  $p$ -wave superconductors“, Phys. Rev. Lett. **86**, 268 (2001).
- <sup>2</sup>A. Y. Kitaev, „Unpaired Majorana fermions in quantum wires“, Phys. Usp. **44**, 131 (2001).
- <sup>3</sup>L. Fu and C. L. Kane, „Superconducting proximity effect and Majorana fermions at the surface of a topological insulator“, Phys. Rev. Lett. **100**, 096407 (2008).
- <sup>4</sup>P. Jordan and E. Wigner, „Über das Paulische Äquivalenzverbot“, Z. Phys. **47**, 631 (1928).
- <sup>5</sup>M. Greiter, V. Schnells and R. Thomale, „The 1D Ising model and the topological phase of the Kitaev chain“, Annals of Physics **351**, 1026 (2014).
- <sup>6</sup>J. Alicea, Y. Oreg, G. Refael, F. von Oppen and M. P. A. Fisher, „Non-Abelian statistics and topological quantum information processing in 1D wire networks“, Nat. Phys. **7**, 412 (2011).
- <sup>7</sup>C. Nayak, S. H. Simon, A. Stern, M. Freedman and S. Das Sarma, „Non-Abelian anyons and topological quantum computation“, Rev. Mod. Phys. **80**, 1083 (2008).
- <sup>8</sup>M. Z. Hasan and C. L. Kane, „Colloquium: topological insulators“, Rev. Mod. Phys. **82**, 3045 (2010).
- <sup>9</sup>T. Karzig, Y. Oreg, G. Refael and M. H. Freedman, „Universal geometric path to a robust Majorana magic gate“, Phys. Rev. X **6**, 031019 (2016).
- <sup>10</sup>L. Fu and C. L. Kane, „Probing neutral majorana fermion edge modes with charge transport“, Phys. Rev. Lett. **102**, 216403 (2009).
- <sup>11</sup>X.-L. Qi and S.-C. Zhang, „Topological insulators and superconductors“, Rev. Mod. Phys. **83**, 1057 (2011).
- <sup>12</sup>C. Chamon, R. Jackiw, Y. Nishida, S.-Y. Pi and L. Santos, „Quantizing Majorana fermions in a superconductor“, Phys. Rev. B **81**, 224515 (2010).
- <sup>13</sup>S. Backens, A. Shnirman, Y. Makhlin, Y. Gefen, J. Mooij and G. Schön, „Emulating Majorana fermions and their braiding by Ising spin chains“, Phys. Rev. B **96**, 195402 (2017).
- <sup>14</sup>S. Backens, A. Shnirman and Y. Makhlin, „Jordan–Wigner transformations for tree structures“, Sci. Rep. **9**, 2598 (2019).
- <sup>15</sup>S. Wang, „Jordan-Wigner transformation in a higher-dimensional lattice“, Phys. Rev. E **51**, 1004 (1995).
- <sup>16</sup>Y. R. Wang, „Ground state of the two-dimensional antiferromagnetic Heisenberg model studied using an extended Wigner-Jordon transformation“, Phys. Rev. B **43**, 3786 (1991).
- <sup>17</sup>F. Verstraete and J. I. Cirac, „Mapping local Hamiltonians of fermions to local Hamiltonians of spins“, J. Stat. Mech. **2005**, P09012 (2005).
- <sup>18</sup>N. Crampé and A. Trombettoni, „Quantum spins on star graphs and the Kondo model“, Nucl. Phys. B **871**, 526 (2013).

- <sup>19</sup>C. J. Bolech and E. Demler, „Observing Majorana bound states in  $p$ -wave superconductors using noise measurements in tunneling experiments“, *Phys. Rev. Lett.* **98**, 237002 (2007).
- <sup>20</sup>J. Nilsson, A. R. Akhmerov and C. W. J. Beenakker, „Splitting of a Cooper pair by a pair of Majorana bound states“, *Phys. Rev. Lett.* **101**, 120403 (2008).
- <sup>21</sup>L. Fu, „Electron teleportation via Majorana bound states in a mesoscopic superconductor“, *Phys. Rev. Lett.* **104**, 056402 (2010).
- <sup>22</sup>A. Zazunov, A. L. Yeyati and R. Egger, „Coulomb blockade of Majorana-fermion-induced transport“, *Phys. Rev. B* **84**, 165440 (2011).
- <sup>23</sup>R. Hützen, A. Zazunov, B. Braunecker, A. L. Yeyati and R. Egger, „Majorana single-charge transistor“, *Phys. Rev. Lett.* **109**, 166403 (2012).
- <sup>24</sup>J. Ulrich and F. Hassler, „Majorana-assisted nonlocal electron transport through a floating topological superconductor“, *Phys. Rev. B* **92**, 075443 (2015).
- <sup>25</sup>Y. Tanaka, T. Yokoyama and N. Nagaosa, „Manipulation of the Majorana fermion, Andreev Reflection, and Josephson current on topological insulators“, *Phys. Rev. Lett.* **103**, 107002 (2009).
- <sup>26</sup>J. Linder, Y. Tanaka, T. Yokoyama, A. Sudbø and N. Nagaosa, „Interplay between superconductivity and ferromagnetism on a topological insulator“, *Phys. Rev. B* **81**, 184525 (2010).
- <sup>27</sup>M. Snelder, M. Veldhorst, A. A. Golubov and A. Brinkman, „Andreev bound states and current-phase relations in three-dimensional topological insulators“, *Phys. Rev. B* **87**, 104507 (2013).
- <sup>28</sup>O. Maistrenko, B. Scharf, D. Manske and E. M. Hankiewicz, „Planar Josephson Hall effect in topological Josephson junctions“, arXiv:2003.05414 [cond-mat.supr-con].
- <sup>29</sup>D. S. Shapiro, A. Shnirman and A. D. Mirlin, „Current-phase relation and  $h/e$ -periodic critical current of a chiral Josephson contact between one-dimensional Majorana modes“, *Phys. Rev. B* **93**, 155411 (2016).
- <sup>30</sup>I. O. Kulik, „Macroscopic quantization and the proximity effect in S-N-S junctions“, *Sov. Phys. JETP* **30**, 944 (1970).
- <sup>31</sup>C. Ishii, „Josephson currents through junctions with normal metal barriers“, *Prog. Theor. Phys.* **44**, 1525 (1970).
- <sup>32</sup>Q. L. He, L. Pan, A. L. Stern, E. C. Burks, X. Che, G. Yin, J. Wang, B. Lian, Q. Zhou, E. S. Choi, K. Murata, X. Kou, Z. Chen, T. Nie, Q. Shao, Y. Fan, S.-C. Zhang, K. Liu, J. Xia and K. L. Wang, „Chiral Majorana fermion modes in a quantum anomalous Hall insulator–superconductor structure“, *Science* **357**, 294 (2017).
- <sup>33</sup>J. Shen, J. Lyu, J. Z. Gao, Y.-M. Xie, C.-Z. Chen, C.-w. Cho, O. Atanov, Z. Chen, K. Liu, Y. J. Hu, K. Y. Yip, S. K. Goh, Q. L. He, L. Pan, K. L. Wang, K. T. Law and R. Lortz, „Spectroscopic fingerprint of chiral Majorana modes at the edge of a quantum anomalous Hall insulator/superconductor heterostructure“, *Proc. Natl. Acad. Sci. USA* **117**, 238 (2020).
- <sup>34</sup>Y. Makhlin, S. Backens and A. Shnirman, „Two-qubit operation on Majorana qubits in ordinary-qubit chains“, *JETP Lett.* **108**, 763 (2018).
- <sup>35</sup>Y. Makhlin, S. Backens and A. Shnirman, „Disentangled quantum operation on Majorana qubits in qubit chains“, *J. Exp. Theor. Phys.* **129**, 733 (2019).
- <sup>36</sup>E. Akkermans, A. Auerbach, J. E. Avron and B. Shapiro, „Relation between persistent currents and the scattering matrix“, *Phys. Rev. Lett.* **66**, 76 (1991).

# Acknowledgements

First of all, I want to thank my adviser *Alexander Shnirman*, who has given me the opportunity to pursue this work and who has accompanied my research journey with his guidance and support since my master studies. In addition, I would like to thank *Yuriy Makhlin* in particular for the collaboration on the subject of Jordan–Wigner transformations and the spin representation of braiding. I am grateful to *Alexander Mirlin*, who agreed to be the second reviewer of this thesis.

Furthermore, I want to thank all *members of TKM* for the very pleasant atmosphere at this institute. There have been many enjoyable and insightful discussions with current and now former colleagues about both physics and non-physics, interesting questions and current events, which I appreciate a lot. I hope that this great community will persist, and I look forward to continuing my work and life at TKM for some more time.

I am very grateful to *my family* for their help, advice and encouragement throughout my life. Their support has been invaluable to me during the creation of this thesis.